Ore Geology Reviews 80 (2017) 1135–1159

Contents lists available at ScienceDirect

Ore Geology Reviews

journal homepage: www.elsevier.com/locate/oregeorev

Cu-Ni-PGE mineralisation at the Aurora Project and potential for a new PGE province in the Northern Bushveld Main Zone

Iain McDonald [a,*], R.E. (Jock) Harmer [b], David A. Holwell [c], Hannah S.R. Hughes [d], Adrian J. Boyce [e]

[a] School of Earth & Ocean Sciences, Cardiff University, Main Building, Park Place, Cardiff CF10 3YE, UK
[b] Department of Geology, Rhodes University, P.O. Box 94, Grahamstown 6140, South Africa
[c] Department of Geology, University of Leicester, University Road, Leicester LE1 7RH, UK
[d] School of Geosciences, University of the Witwatersrand, P.O. Wits, 2050, South Africa
[e] Scottish Universities Environmental Research Centre, Rankine Avenue, East Kilbride G75 0QF, UK

ARTICLE INFO

Article history:
Received 25 July 2016
Received in revised form 6 September 2016
Accepted 12 September 2016
Available online 13 September 2016

Keywords:
Bushveld Complex
Northern limb
Base metal sulphides
Main Zone
Pigeonite
Fractional crystallisation

ABSTRACT

The Aurora Project is a Cu-Ni-PGE magmatic sulphide deposit in the northern limb of the Bushveld Complex of South Africa. Since 1992 mining in the northern limb has focussed on the Platreef deposit, located along the margin of the complex. Aurora has previously been suggested to represent a far-northern facies of the Platreef located along the basal margin of the complex and this study provides new data with which to test this assertion. In contrast to the Platreef, the base metal sulphide mineralisation at Aurora is both Cu-rich (Ni/Cu <1) and Au-rich. The sulphides are hosted predominantly in leucocratic rocks (gabbronorites and leucogabbronorites) with low Cr/MgO (<30) where pigeonite and orthopyroxene co-exist as low-Ca pyroxenes without cumulus magnetite. This mineral association is found in the Upper Main Zone and the Aurora mineral chemistry is consistent with this stratigraphic interval. Pigeonite gabbronorites above the Aurora mineralisation have high Cu/Pd ratios (>50,000) reflecting the preferential removal of Pd over Cu in the sulphides below. Similarly high Cu/Pd ratios characterise the Upper Main Zone in the northern limb above the pigeonite + orthopyroxene interval and suggest that Aurora-style sulphide mineralisation may be developed here as well. The same mineralogy and geochemical features also appear to be present in the T Zone of the Waterberg PGE deposit, located under younger cover rocks to the north of Aurora. If these links are proved they indicate the potential for a previously unsuspected zone of Cu-Ni-PGE mineralisation extending for over 40 km along strike through the Upper Main Zone of the northern Bushveld.

1. Introduction

The northern limb of the Bushveld Complex of South Africa is one of the most significant mineral provinces for magmatic sulphide deposits containing Ni, Cu and the platinum-group elements (PGE) as it hosts the Platreef, one of the world's largest primary PGE deposits (see reviews in Kinnaird et al., 2005; McDonald and Holwell, 2011 and Kinnaird and Nex, 2015). Unlike the thin (0.3–2 m thick) and stratiform reef-type deposits such as the Merensky Reef and the UG2 chromitite of the eastern and western Bushveld that have traditionally relied on narrow mining methods, the Platreef comprises a 10–200 m wide mineralized zone of pyroxenites, gabbronorites and norites that are amenable to open pit mining (White, 1994; Bye and Bell, 2001). Anglo Platinum's Mogalakwena mine complex that extracts and processes Platreef ore is one of the lowest-cost (per PGE ounce) PGE mining operations in the world and its success, coupled with rising costs and limited scope for mechanization associated with deep Merensky Reef and UG2-type deposits, have led to concerted exploration for similar Ni-Cu-PGE orebodies at surface or at reasonably shallow depths elsewhere in the northern limb of the Bushveld Complex.

This search has included exploration and evaluation of potential Ni-Cu-PGE deposits where the associations and genetic links with stratiform reef-type or Platreef-style mineralisation are not immediately clear, and in parts of the magmatic stratigraphy where the potential for Ni-Cu-PGE has traditionally been thought to be low (see recent reviews by Maier et al., 2013; and Kinnaird and Nex, 2015). The purpose of this paper is to provide a comprehensive description of one of these poorly understood deposits, known as the Aurora Project, to compare and contrast it with established Platreef-style deposits and to consider its wider significance for the development of Ni-Cu-PGE mineralisation in the northern Bushveld Complex.

* Corresponding author.
E-mail addresses: mcdonaldi1@cardiff.ac.uk (I. McDonald), J.Harmer@ru.ac.za (R.E.(J.) Harmer), dah29@leicester.ac.uk (D.A. Holwell), hannah.hughes@wits.ac.za (H.S.R. Hughes), Adrian.Boyce@glasgow.ac.uk (A.J. Boyce).

http://dx.doi.org/10.1016/j.oregeorev.2016.09.016

1.1. Regional geology

The Bushveld Complex comprises the mafic-ultramafic Rustenburg Layered Suite (RLS; South African Committee for Stratigraphy, 1980) and a felsic portion made up of the Rashoop Granophyre and the Bushveld Granites. The rhyolitic lavas that constitute the upper part of the overlying Rooiberg Group, although not designated as part of the Bushveld Complex, may in part be coeval with the Bushveld cumulate rocks and may have formed a low-density carapace over the RLS as the mafic magma intruded (Kruger, 2005; VanTongeren et al., 2016). The RLS is subdivided into 5 limbs: far western, western, eastern, northern and the southern (Bethal) limb that is largely obscured by cover rocks. In the northern limb, the RLS is intruded into late Archaean and early Proterozoic (2.7–2.1 Ga) sediments of the Transvaal Supergroup and older Archaean granite-gneiss basement (Fig. 1). The RLS is conventionally divided into five zones comprising: a Marginal Zone of norites; Lower Zone pyroxenites and harzburgites; Critical Zone chromitite-pyroxenite-norite cyclic units; Main Zone gabbronorites; and Upper Zone anorthosites, gabbros and magnetitites (Eales and Cawthorn, 1996). However key elements of stratigraphy within the RLS that can be traced across the eastern and western limbs (e.g. the Pyroxenite Marker interval and the whole of the Lower Critical Zone) are apparently absent from the northern limb (Van der Merwe, 1976; Ashwal et al., 2005; Tanner et al., 2014). Similarly, other stratigraphic markers such as a thick zone of troctolite and olivine gabbronorite in the Main Zone (referred to here as the Troctolite Unit) and a pronounced hiatus between the Platreef and base of the Main Zone are not recognised in the eastern and western limbs and appear to be unique to the northern

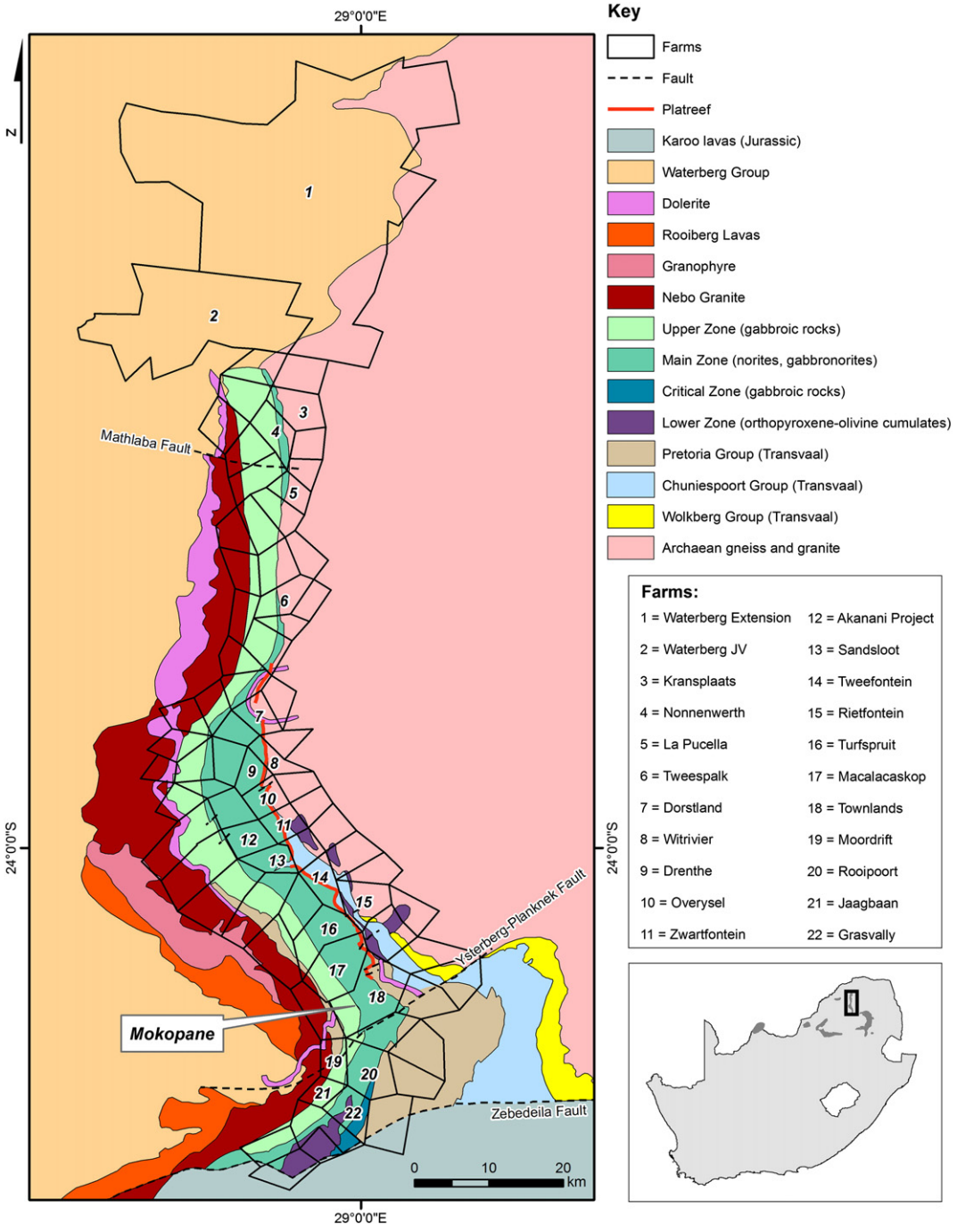

Fig. 1. Northern limb map showing the geology and the localities discussed in the text.

limb (Van der Merwe, 1976; Ashwal et al., 2005; Holwell et al., 2005; Holwell and Jordaan, 2006; Tanner et al., 2014). For these reasons, direct stratigraphic comparisons between the northern limb and the rest of the Bushveld Complex south of the Thabazimbi-Murchison lineament remain unclear (McDonald et al., 2005; Van der Merwe, 2008; McDonald and Holwell, 2011; Yudovskaya et al., 2013; Kinnaird and Nex, 2015).

1.2. The Platreef

The Platreef (sensu stricto; as defined by Kinnaird and McDonald, 2005) is developed north of the town of Mokopane as a 10–400 m thick package of generally pyroxenitic lithologies with PGE and Ni-Cu base-metal sulphide (BMS) mineralisation, located at the base of the RLS and overlain by norites and gabbronorites assigned to the Main Zone. As the Platreef strikes northwards from Mokopane it rests upon a succession of progressively older units of the Transvaal Supergroup: quartzites and shales of the Silverton and Timeball Hill Formations; shales of the Duitschland Formation; the Penge banded iron formation; dolomites of the Malmani Subgroup; and finally on the farm Zwartfontein, the Platreef rests on Archaean basement granites and gneisses. Under this definition, Platreef (sensu stricto) is recognised to extend for approximately 40 km from the farm Townlands to the farm Dorstland (Fig. 1; McDonald and Holwell, 2011).

Holwell et al. (2005) and Holwell and Jordaan (2006) recognised and mapped the effects of chilling, erosion of the Platreef and incorporation of Platreef xenoliths by the overlying Main Zone. The latter is a fundamental observation because it demonstrates that emplacement of the Main Zone magma in the northern Bushveld significantly post-dates the Platreef and consequently the Main Zone magma could not have contributed metals to the Platreef. The undepleted chalcophile element budget of the Main Zone magma could thus have been concentrated elsewhere into distinct Ni-Cu-PGE deposits within the northern limb Main Zone as it developed (McDonald and Holwell, 2011; Holwell et al., 2013). This situation contrasts with the eastern and western limbs of the Bushveld, where the Main Zone magma is believed to have been involved in the formation of the Merensky Reef (Maier et al., 1996; Seabrook et al., 2005; Kruger, 2005). As a consequence, the Main Zone in the eastern and western Bushveld Complex is considered to be barren of magmatic sulphide mineralisation (Lee, 1996; Barnes and Maier, 2002; Maier et al., 2013).

1.3. Main Zone-hosted Ni-Cu-PGE mineralisation

In the northern limb, magmatic sulphide mineralisation has been found within cumulates that are considered part of the Main Zone. The most southerly deposit of this type occurs on the farm Moorddrift (Fig. 1) where Ni-Cu-PGE mineralisation is hosted in leucogabbronorites and a melagabbronorite/pyroxenite succession in the Upper Main Zone (Maier and Barnes, 2010; Holwell et al., 2013). The second example of this mineralisation is the recently discovered Waterberg Ni-Cu-PGE deposit (Fig. 1) that lies under a cover sequence of post-Bushveld Waterberg Group sediments beyond the previously known northern extent of the northern limb (Lomberg, 2012, 2013; Huthmann et al., 2016). The rocks that host the Waterberg mineralisation produce U-Pb zircon ages of 2059 ± 3 and 2053 ± 5 Ma (Huthmann et al., 2016) that overlap with the high precision zircon age of 2056 ± 1 Ma for different zones within the RLS (Zeh et al., 2015). This age, coupled with a magnetite-rich upper portion of the stratigraphy at Waterberg that resembles the Upper Zone of the RLS, suggests that Waterberg is hosted within a far northern extension of the northern Bushveld that is developed for at least another 30 km under the post-Bushveld cover sediments of the Waterberg Group (Huthmann et al., 2016).

Immediately south of the Waterberg deposit is the Aurora Project (Fig. 1) which comprises a group of 7 farms (Altona 696LR, Kransplaats 422LR, La Pucella 69LR, Luge 697LR, Nonnenwerth 421LR, Non Plus Ultra 683LR and Schaffhausen 698LR). Mineralisation is developed in a narrow belt close to the base of the RLS and the basement granite-gneiss immediately north of the major transgression where Upper Zone cumulates cut across the Main Zone layers and are in direct contact with the granite-gneiss floor (Van der Merwe, 1976; Fig. 1). The Aurora mineralisation was first recognised from soil geochemical anomalies for Cu and Ni and between 1974 and 1992 Union Corporation and Genmin drilled 43 boreholes on the farm Nonnenwerth (Venmyn-Rand, 2010) to confirm the deposit. Between 2002 and 2010, the Aurora Project was expanded and developed by Pan Palladium Ltd., which drilled a further 92 boreholes across 18 km of strike on Kransplaats, Nonnenwerth, Altona and La Pucella (Fig. 2) to define a JORC-compliant, inferred resource of 125 Mt of sulphide ore at 1.34 g/t Pt + Pd + Au, 0.08% Cu and 0.05% Ni (Venmyn-Rand, 2010). Within this resource, local higher grade target zones were identified (Fig. 2). Target Zone 1 in the northern portion of the farm La Pucella 69LR has the highest average PGE grade, with three broadly stratiform zones of mineralisation that can be traced along strike and down dip (Fig. 3), and is considered to have the best potential for development as a mining project. In 2010, the Aurora Project was acquired by Sylvania Resources Ltd. and currently forms part of their portfolio of northern Bushveld PGE projects (Venmyn-Rand, 2010).

The Aurora mineralisation is shown on regional geological maps as being hosted within gabbronorites of the Main Zone (van der Merwe, 1976; Fig. 2). The earliest publically available descriptions were provided by Harmer et al. (2004) who highlighted the fact that mineralisation was hosted by anorthosites and leucogabbronorites rather than ultramafic rocks. Manyeruke (2007) studied two of the Genmin boreholes (2121 and 2199; Fig. 2) from Nonnenwerth and divided the stratigraphy into “Platreef” and “Main Zone”; separated by an extensive raft or xenolith of calc-silicate that was identified in both boreholes. The deposit is also described as Platreef by Maier et al. (2008) who contended that Aurora represents a northern contact facies that is an extension of the Platreef (sensu-stricto). McDonald and Harmer (2010) disputed this and argued on petrological and geochemical grounds that the mineralized rocks at Aurora were part of the Main Zone. They also noted that the Aurora metals budget was significantly more Cu-rich and Au-rich than equivalent published mineral resources for the Platreef (Fig. 4).

The purpose of this paper is to provide a detailed description of the stratigraphy, geochemistry and mineralogy of the Aurora mineralisation. This will allow us to address the critical question of whether Aurora is part of the Platreef or part of the northern Main Zone. Further, if it is part of the Main Zone, how Aurora may relate to the wider stratigraphy and mineralogy of the Main Zone at the Waterberg Project, Moorddrift and elsewhere?

2. Samples and methods

Quarter core samples (20–25 cm in length) were selected from boreholes LAP-04, LAP-29 and LAP-31 that occur in Target Zone 1 on La Pucella 69LR (Fig. 3). Pan Palladium geologists originally logged these boreholes as comprising a suite of gabbros, feldspathic gabbros, “spotted gabbros” and harzburgites. The logs were re-examined and the rock units reclassified using IUGS terminology in the light of the petrographic work carried out in this study. Representative images of the major lithological units and their relationships are given in Fig. 5. LAP-04 was used to study a number of complex relationships between coarse-grained leucogabbronorite veins and ultramafic rocks at the base of the sequence (Fig. 5c and d) and full logging of this borehole was not attempted. Pan Palladium Ltd. assayed half core samples every metre for Pt, Pd and Au using Pb fire assay and for a suite of trace elements (Cr, V, S, Ni, Cu, Rb and Sr) by X-ray Fluorescence (XRF). These assays were carried out at Set Point Laboratories in Johannesburg.

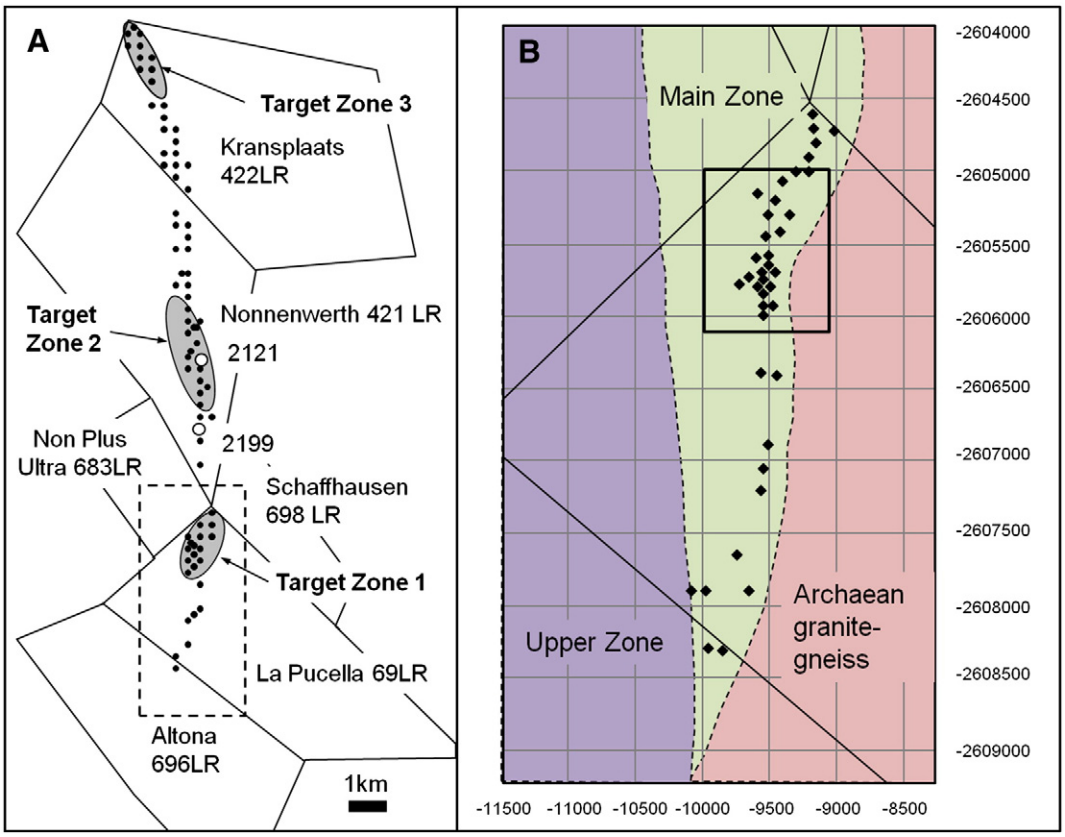

Fig. 2. (A) Location of Target Zones 1–3 across the Aurora Project. (B) Inset from (A) showing the geology and locations of boreholes from Target Zone 1 on northern La Pucella.

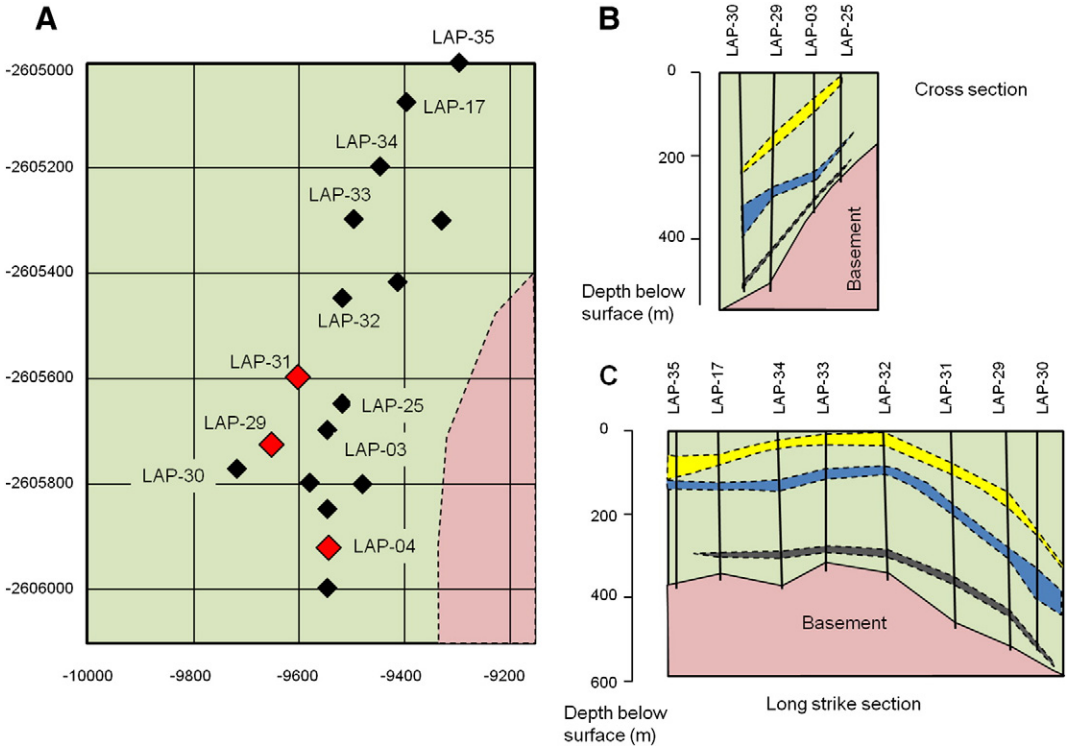

Fig. 3. (A) Detailed positions of boreholes used in the study. The lithological colour scheme is the same as for Fig. 2. (B) Cross section down dip to highlight the positions of the three zones of elevated PGE grade (shown by hatched lines) observed in Target Zone 1 boreholes. (C) Strike section showing the same zones of elevated PGE grade. Diagram redrawn from Kinnaird and Nex (2015).

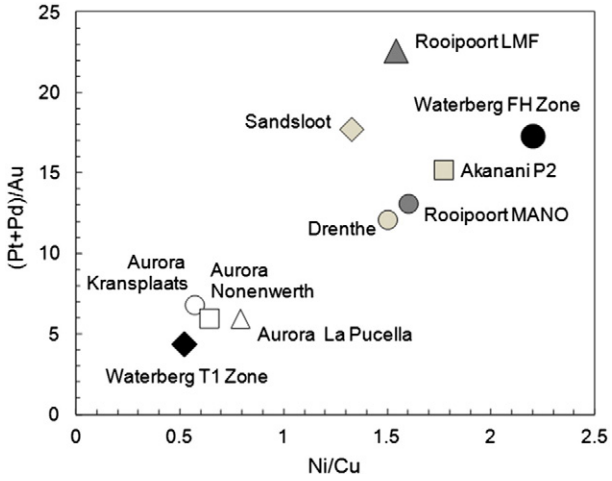

Fig. 4. Metal ratios for Aurora mineral resources compared with the Platreef and the Waterberg deposit. The resource information for Waterberg is from Lomberg (2013). All other information is from McDonald and Holwell (2011).

3–4 cm long and 1 cm thick portions of the quarter core samples from LAP-04, LAP-29 and LAP-31 were cut and prepared as polished thin sections for transmitted and reflected light microscopy at Cardiff University. All of the remaining quarter core sample was crushed to chips in a Mn steel jaw-crusher and then milled to a fine powder in an agate planetary ball mill. Loss on Ignition (LOI) was determined gravimetrically. Major and trace elements were measured by inductively coupled plasma optical emission spectrometry (ICP-OES) and inductively coupled plasma mass spectrometry (ICP-MS) using methods and instrumentation described by McDonald and Viljoen (2006). Analysis for 6 PGE and Au was carried out by Ni-sulphide fire assay followed by Te co-precipitation and ICP-MS (Huber et al., 2001; McDonald and Viljoen, 2006). Major and trace element data and noble metal data are given in Tables 1 and 2 respectively. Accuracy was constrained by analysis of the certified international reference materials TDB1, WPR1 and WMG1 for PGE and Au, and JB1a, NIM-P and NIM-N for all other trace and major elements (see Supplementary Table S1). Precision for PGE analysis was estimated by repeat analysis of a sub-set of samples (Supplementary Table S2).

Further thin-section examination and quantitative microanalysis was carried out on a Cambridge Instruments S360 scanning election microscope (SEM) at Cardiff University. Quantitative microanalyses were obtained using an Oxford Instruments INCA Energy EDX analyser attached to the SEM, with operating conditions set at 20 kV and specimen calibration current of ~2 nA at a fixed working distance of 25 mm. Analytical drift checks were carried out every 2 h using the Co reference standard and a comprehensive suite of standards from MicroAnalysis Consultants Ltd. were used to calibrate the EDX analyser.

Laser ablation-inductively coupled plasma-mass spectrometry (LA-ICP-MS) analyses were performed on plagioclase and pyroxenes using a New Wave Research UP213 laser system coupled to a Thermo X Series 2 ICP-MS. The laser was operated using a frequency of 10 Hz that developed pulse energy of 3–4 mJ for a 40 μm diameter beam. The time-resolved LA-ICP-MS analysis involved an acquisition time of 90 s; comprising a 20 s gas blank, 60 s line ablation and 10 s wash-out. Calibration of the ICP-MS was accomplished using the USGS glass standards BIR-2G and BHVO-2G with USGS basalt glass BCR-2G analysed as an unknown every 10–15 samples to check the accuracy of the analysis. A summary of the measured concentrations in the BCR-2 g unknowns versus expected concentrations are given in Supplementary Table S3.

The isotopes analysed were ^{23}Na, ^{25}Mg, ^{29}Si, ^{39}K, ^{44}Ca, ^{47}Ti, ^{51}V, ^{52}Cr, ^{55}Mn, ^{60}Ni, ^{71}Ga, ^{85}Rb, ^{88}Sr, ^{89}Y, ^{90}Zr, ^{137}Ba, ^{139}La, ^{140}Ce, ^{141}Pr, ^{146}Nd, ^{147}Sm, ^{153}Eu and ^{208}Pb. Silicon concentrations, as determined using SEM, were used as an internal standard to correct for instrumental drift. Blank correction, drift corrections and conversion of ICP-MS output data (counts/s) to concentrations (wt% or μg/g) were accomplished using the Thermo Plasmalab software. Major and trace element concentrations of plagioclase, low-Ca pyroxene, clinopyroxene and olivine are given in Supplementary Tables S4–S7.

Whole-rock sulphur isotope analysis was carried out on a limited number of samples using the methods described by Hughes et al. (2015). SO_2 gases were analysed using a ThermoFisher Scientific MAT 253 dual inlet mass spectrometer. Standards used throughout all

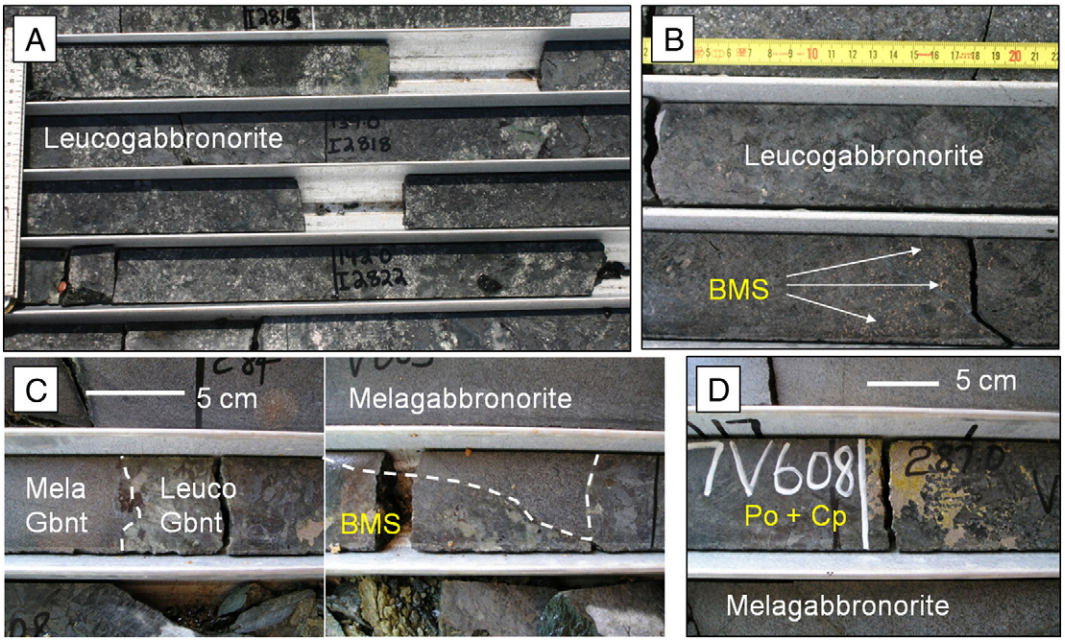

Fig. 5. Representative pictures of different lithologies at La Pucella. (A) LAP 29; dark, vari-textured leucogabbronorites. (B) LAP 31; coarse grained leucogabbronorite with disseminated base metal sulphides (BMS). (C) LAP-04; coarse grained leucogabbronorite vein with sulphides in medium grained melagabbronorite. Sharp contacts are indicated with a dashed line; (D) LAP-04; patches of massive and net-textured pyrrhotite (Po) and chalcopyrite (Cp) in a coarse grained gabbronorite intruded into medium grained melagabbronorites.

Table 1
Major and trace element data for Aurora samples.

Sample		P-1	P-2	P-3	P-4	P-5	P-6	P-7	P-8	P-9	P-10	P-11	P-12	P-13	P-14	P-15	P-16	CDF13A
Borehole		LAP-29	LAP-29	LAP-29	LAP-29	LAP-29	LAP-29	LAP-29	LAP-29	LAP-29	LAP-29	LAP-29	LAP-29	LAP-29	LAP-29	LAP-29	LAP-29	LAP-29
Depth (m)		-39.85	-80.15	-144.90	-146.95	-150.10	-194.86	-243.17	-259.77	-266.05	-267.95	-270.23	-275.15	-280.05	-284.86	-390.19	-414.78	-418.17
Rock Unit		3	3	2	2	2	2	4	2	2	2	2	2	2	2	1	2	2
Lithology		MeGbn	MeGbn	LGbn	MeGbn	LGbn	Ol Gbnt	Mgt Gb	LGbn	LGbn	LGbn	LGbn	LGbn	MeGbn	MeGbn	MelGbn	MeGbn	MeGbn
SiO2	wt%	48.31	51.07	48.47	51.91	48.17	51.07	49.28	49.18	48.49	49.37	46.85	47.99	48.56	50.63	52.32	52.95	49.95
TiO2	wt%	0.31	0.34	0.20	0.22	0.08	0.09	2.00	0.08	0.10	0.23	0.06	0.16	0.14	0.16	0.17	0.64	0.16
Al2O3	wt%	14.26	12.35	21.32	9.36	30.88	16.19	5.02	27.83	30.22	25.09	29.52	29.61	17.32	16.95	9.06	11.98	12.96
Fe2O3	wt%	10.63	12.13	6.99	14.71	2.00	9.14	21.76	3.81	2.44	5.72	2.33	4.08	9.31	7.29	9.99	11.06	10.33
MnO	wt%	0.20	0.23	0.11	0.26	0.03	0.13	0.32	0.07	0.05	0.09	0.05	0.05	0.14	0.14	0.21	0.32	0.20
MgO	wt%	9.62	10.79	7.11	15.01	1.26	9.04	10.58	3.83	1.67	3.83	1.59	1.79	8.77	9.30	14.24	10.10	9.69
CaO	wt%	10.99	9.72	11.96	6.30	13.95	11.14	10.13	13.50	13.40	11.98	12.98	13.01	12.94	13.18	12.61	10.53	11.56
Na2O	wt%	1.71	1.10	1.34	0.91	2.19	2.08	0.67	2.11	2.24	2.28	2.90	2.09	1.18	0.98	0.40	0.85	1.59
K2O	wt%	0.09	0.13	0.08	0.12	0.09	0.09	0.03	0.07	0.07	0.13	0.42	0.14	0.04	0.05	0.04	0.14	0.14
P2O5	wt%	0.01	0.02	0.01	0.02	0.00	0.02	0.21	0.00	0.01	0.02	0.01	0.00	0.01	0.01	0.01	0.04	0.00
LOI	wt%	3.70	1.40	2.40	0.79	1.67	2.22	0.77	0.69	0.60	1.07	2.83	1.18	0.84	0.75	0.41	1.06	2.73
Total	wt%	99.83	99.26	99.99	99.62	100.33	101.20	100.77	101.17	99.29	99.82	99.54	100.10	99.26	99.42	99.47	99.66	99.32
Sc	ppm	44.0	42.2	20.9	38.0	6.0	9.0	70.3	12.5	5.6	11.0	4.4	6.8	32.4	36.9	50.6	43.1	45.0
V	ppm	178.8	184.5	90.8	130.3	24.7	16.8	744.3	21.6	8.4	45.3	19.6	22.5	92.3	108.4	148.7	236.1	162.7
Cr	ppm	212.3	267.6	191.5	312.4	49.1	35.2	133.8	58.2	4.0	25.1	61.3	8.0	119.1	89.9	941.9	84.1	79.9
Co	ppm	54.6	66.0	38.1	75.2	11.4	69.3	88.5	16.9	9.6	29.5	14.9	30.9	92.7	40.1	59.9	151.4	65.6
Zn	ppm	92.7	96.4	49.0	67.0	31.4	84.7	108.3	25.9	17.5	41.2	32.0	16.7	116.6	65.1	93.3	285.7	74.2
Ga	ppm	13.3	12.2	14.5	9.4	17.8	17.4	11.1	19.7	18.0	17.2	17.1	18.9	12.1	12.1	7.9	9.9	10.5
Rb	ppm	0.2	0.8	0.1	1.0	0.1	0.3	0.1	0.1	0.1	0.9	6.1	0.7	0.1	0.1	0.1	1.5	2.2
Sr	ppm	154.8	150.4	196.2	96.4	283.7	241.0	96.8	267.6	295.6	275.1	391.9	298.2	163.7	164.1	92.5	83.1	131.8
Y	ppm	10.4	10.0	3.8	6.4	1.6	2.1	29.0	2.6	2.2	3.8	1.6	2.4	5.3	6.8	6.7	17.9	5.6
Zr	ppm	12.3	11.5	5.6	6.3	4.4	4.8	14.3	6.0	5.2	6.8	4.6	6.5	6.9	6.0	5.0	13.8	7.6
Nb	ppm	0.43	0.62	0.59	0.46	0.52	0.55	1.13	0.46	0.57	0.74	0.47	0.83	0.57	0.49	0.42	1.57	0.41
Ba	ppm	32.60	43.86	35.15	44.99	56.57	40.04	21.79	37.47	52.87	103.39	94.74	79.91	25.93	27.34	9.75	37.45	36.06
La	ppm	1.50	1.91	1.01	1.39	1.36	1.97	4.42	1.52	1.62	2.35	1.37	1.42	1.35	1.14	1.23	2.59	0.98
Ce	ppm	4.17	4.42	2.86	3.30	3.28	3.14	14.16	3.29	3.78	6.03	3.39	3.80	2.63	3.13	2.59	7.33	2.20
Pr	ppm	0.65	0.67	0.37	0.44	0.38	0.37	2.38	0.39	0.45	0.71	0.41	0.44	0.37	0.45	0.39	1.11	0.34
Nd	ppm	3.11	3.07	1.52	1.85	1.37	1.44	11.28	1.56	1.73	2.57	1.51	1.66	1.63	1.92	1.79	4.95	1.53
Sm	ppm	0.96	0.93	0.40	0.54	0.27	0.33	3.59	0.36	0.38	0.54	0.30	0.34	0.50	0.58	0.61	1.61	0.52
Eu	ppm	0.45	0.41	0.31	0.23	0.42	0.34	0.58	0.39	0.36	0.43	0.36	0.41	0.28	0.30	0.22	0.27	0.30
Gd	ppm	1.22	1.18	0.51	0.69	0.28	0.39	4.08	0.42	0.41	0.61	0.31	0.38	0.62	0.73	0.74	1.94	0.62
Tb	ppm	0.22	0.21	0.09	0.12	0.04	0.06	0.69	0.07	0.06	0.10	0.05	0.06	0.11	0.13	0.14	0.35	0.12
Dy	ppm	1.59	1.50	0.67	0.91	0.29	0.43	4.69	0.50	0.44	0.64	0.31	0.41	0.79	0.96	0.97	2.55	0.89
Ho	ppm	0.34	0.33	0.14	0.20	0.06	0.09	0.95	0.11	0.09	0.14	0.07	0.08	0.18	0.20	0.21	0.54	0.18
Er	ppm	1.03	0.98	0.44	0.63	0.17	0.27	2.76	0.33	0.29	0.43	0.19	0.24	0.53	0.63	0.63	1.64	0.60
Tm	ppm	0.16	0.16	0.07	0.10	0.03	0.04	0.41	0.05	0.04	0.07	0.03	0.04	0.08	0.09	0.10	0.26	0.10
Yb	ppm	1.09	1.10	0.46	0.76	0.16	0.31	2.75	0.35	0.29	0.49	0.20	0.26	0.55	0.66	0.67	1.92	0.67
Lu	ppm	0.17	0.16	0.07	0.12	0.02	0.04	0.41	0.05	0.04	0.07	0.03	0.03	0.08	0.10	0.10	0.30	0.11
Hf	ppm	0.33	0.34	0.14	0.17	0.08	0.12	0.52	0.12	0.12	0.19	0.09	0.16	0.15	0.15	0.11	0.45	0.19
Ta	ppm	0.02	0.03	0.02	0.02	0.02	0.02	0.06	0.02	0.03	0.04	0.02	0.04	0.02	0.02	0.03	0.11	0.02
Th	ppm	0.08	0.19	0.13	0.20	0.13	0.16	0.27	0.13	0.25	0.77	0.13	0.20	0.13	0.17	0.24	0.71	0.05
U	ppm	0.02	0.05	0.03	0.06	0.03	0.05	0.18	0.04	0.06	0.10	0.04	0.08	0.04	0.04	0.07	0.44	0.02
Cr/MgO		22.07	24.79	26.92	20.81	38.84	3.89	12.65	15.21	2.37	6.55	38.47	4.48	13.57	9.67	66.16	8.33	8.24
CaO/Al2O3		0.77	0.79	0.56	0.67	0.45	0.69	2.02	0.48	0.44	0.48	0.44	0.44	0.75	0.78	1.39	0.88	0.89
V/Cr		0.84	0.69	0.47	0.42	0.50	0.48	5.56	0.37	2.13	1.81	0.32	2.81	0.78	1.21	0.16	2.81	2.04

Sample	CDF13B	CDF15	P-17	P-18	N-1	N-2	N-3	N-4	N-5	N-6	N-7	N-8	N-9	N-10	N-11	N-12	N-13	CDF08
Borehole	LAP-29	LAP-29	LAP-29	LAP-29	LAP-31	LAP-31	LAP-31	LAP-31	LAP-31	LAP-31	LAP-31	LAP-31	LAP-31	LAP-31	LAP-31	LAP-31	LAP-31	LAP-31
Depth (m)	-418.27	-431.89	-460.31	-479.88	-25.45	-70.23	-80.42	-81.97	-87.50	-100.05	-164.89	-170.31	-174.88	-179.79	-205.05	-254.78	-310.11	-324.66
Rock Unit	2	1	1	1	3	2	2	2	2	2	2	2	2	2	4	2	1	1
Lithology	MeGbn	Web	Web	MelGbn	MeGbn	LGbn	LGbn	LGbn	LGbn	LGbn	LGbn	LGbn	Ol Gbn	LGbn	Mgt Gb	MeGbn	MelGbn	Perid
SiO2	51.36	53.90	54.33	56.67	50.21	49.51	49.33	49.67	49.27	49.19	46.02	47.82	44.77	48.58	36.70	51.59	49.40	53.31
TiO2	0.16	0.17	0.13	0.19	0.28	0.09	0.06	0.10	0.07	0.16	0.10	0.07	0.09	0.08	4.13	0.16	0.17	0.16
Al2O3	13.15	3.56	5.53	5.28	18.62	25.71	29.79	29.75	30.06	28.87	27.85	29.23	10.92	25.06	4.52	14.73	12.16	3.35
Fe2O3	10.25	10.83	11.18	9.44	8.49	3.71	2.97	2.33	2.98	2.31	3.63	3.56	15.69	3.60	32.77	8.20	9.97	12.61
MnO	0.16	0.21	0.24	0.23	0.15	0.07	0.04	0.04	0.04	0.04	0.04	0.05	0.18	0.07	0.28	0.17	0.19	0.20
MgO	8.90	21.85	20.63	17.79	7.45	3.57	2.23	1.54	1.98	1.86	1.62	2.69	16.35	4.40	9.58	10.21	14.49	23.61
CaO	11.47	7.89	6.59	8.73	11.35	12.21	12.77	13.43	14.17	13.56	12.52	11.95	5.42	13.81	12.53	12.61	8.35	5.36
Na2O	1.64	0.37	0.58	0.60	2.20	2.72	2.76	2.63	2.06	2.19	2.47	2.75	0.81	2.27	0.60	1.51	0.16	0.40
K2O	0.15	0.03	0.01	0.14	0.09	0.16	0.19	0.11	0.05	0.08	0.15	0.16	0.09	0.10	0.09	0.08	0.00	0.05
P2O5	0.01	0.00	0.02	0.02	0.01	0.01	0.00	0.01	0.01	0.01	0.00	0.01	0.02	0.01	0.30	0.01	0.01	0.00
LOI	1.89	0.99	0.53	0.24	0.21	2.00	0.85	0.78	0.52	0.72	6.00	1.74	6.12	1.53	-0.29	0.83	6.35	0.29
Total	99.14	99.82	99.75	99.31	99.05	99.75	101.00	100.38	101.22	98.99	100.40	100.03	100.47	99.51	101.22	100.11	101.26	99.33
Sc	41.6	45.8	34.1	43.2	29.2	12.3	4.2	5.8	8.2	9.7	6.5	4.2	14.4	19.8	73.4	41.0	48.7	29.0
V	174.4	154.6	81.4	83.2	125.2	26.7	24.0	9.7	17.8	35.0	18.8	18.3	26.7	45.3	1067.4	121.9	150.7	118.0
Cr	64.1	1547.1	1992.4	1419.7	171.9	56.0	11.9	26.0	39.7	41.1	34.8	6.7	52.5	65.4	114.9	169.2	1380.7	1768.0
Co	62.2	83.0	70.0	62.2	39.7	18.7	19.7	12.2	18.0	10.1	38.4	10.3	141.9	17.4	141.2	46.1	91.7	90.5
Zn	65.3	66.5	83.5	110.0	56.0	39.1	21.1	26.1	16.5	14.3	45.7	25.1	103.1	46.1	278.3	64.1	67.9	89.1
Ga	10.2	4.8	7.5	8.3	15.3	16.4	19.9	17.9	17.3	17.3	16.6	18.4	8.8	15.2	19.3	11.6	6.5	4.9
Rb	2.6	0.7	0.6	1.6	0.1	0.6	0.6	0.0	0.1	0.0	0.4	0.6	1.5	0.4	1.3	0.4	0.1	0.7
Sr	123.5	24.2	79.7	144.1	224.9	282.5	317.8	306.5	284.3	271.4	286.3	370.4	86.0	329.4	50.8	154.5	22.6	27.4
Y	6.3	5.8	5.6	16.2	6.7	2.4	1.1	1.5	2.0	2.5	1.4	1.1	1.9	3.2	26.1	6.3	6.4	4.5
Zr	7.4	18.7	11.1	14.1	10.8	3.7	4.7	3.7	6.3	4.5	1.8	2.5	4.0	3.7	27.6	5.4	5.3	5.4
Nb	0.43	0.67	0.84	0.82	0.57	0.43	0.42	0.44	0.48	0.53	0.44	0.41	0.39	0.37	2.01	0.40	0.40	0.39
Ba	36.28	15.43	33.76	56.92	61.28	74.23	79.46	69.93	54.10	63.16	67.11	78.24	10.52	50.56	14.88	26.00	5.33	11.67
La	1.30	0.98	1.29	4.66	1.71	1.87	1.25	1.05	1.68	1.90	1.35	1.68	0.80	0.78	1.76	1.09	1.14	0.61
Ce	2.98	2.41	4.48	11.67	4.23	3.46	3.62	3.28	3.26	4.17	2.76	3.84	2.16	2.54	8.04	2.73	2.44	1.56
Pr	0.43	0.37	0.59	1.75	0.60	0.42	0.40	0.38	0.38	0.48	0.32	0.43	0.26	0.33	1.43	0.40	0.35	0.23
Nd	1.93	1.64	2.39	7.61	2.57	1.55	1.40	1.35	1.44	1.81	1.17	1.51	1.01	1.35	7.15	1.79	1.62	1.06
Sm	0.61	0.55	0.67	2.20	0.74	0.34	0.27	0.28	0.32	0.40	0.25	0.28	0.24	0.37	2.39	0.54	0.53	0.38
Eu	0.30	0.17	0.18	0.52	0.46	0.45	0.49	0.43	0.41	0.45	0.40	0.54	0.16	0.35	0.43	0.29	0.20	0.14
Gd	0.71	0.64	0.76	2.31	0.86	0.37	0.23	0.30	0.34	0.42	0.25	0.30	0.29	0.41	3.03	0.72	0.68	0.45
Tb	0.14	0.12	0.14	0.38	0.16	0.06	0.04	0.04	0.05	0.07	0.04	0.04	0.05	0.08	0.54	0.13	0.13	0.09
Dy	1.01	0.92	0.92	2.46	1.10	0.41	0.24	0.31	0.36	0.44	0.28	0.27	0.35	0.53	3.77	0.93	0.96	0.69
Ho	0.21	0.19	0.20	0.49	0.24	0.09	0.05	0.06	0.08	0.09	0.06	0.05	0.08	0.11	0.77	0.20	0.21	0.15
Er	0.69	0.63	0.60	1.39	0.69	0.26	0.13	0.18	0.22	0.26	0.16	0.14	0.24	0.34	2.18	0.63	0.67	0.50
Tm	0.11	0.10	0.09	0.21	0.11	0.04	0.02	0.03	0.03	0.04	0.02	0.02	0.04	0.05	0.31	0.09	0.10	0.09
Yb	0.77	0.67	0.70	1.46	0.74	0.26	0.16	0.17	0.23	0.26	0.16	0.14	0.31	0.34	2.07	0.65	0.77	0.59
Lu	0.13	0.11	0.13	0.22	0.11	0.04	0.03	0.02	0.03	0.04	0.02	0.02	0.05	0.05	0.31	0.10	0.12	0.10
Hf	0.18	0.47	0.29	0.41	0.25	0.05	0.06	0.05	0.11	0.09	0.05	0.04	0.07	0.07	1.09	0.17	0.12	0.14
Ta	0.02	0.03	0.05	0.06	0.03	0.02	0.02	0.03	0.03	0.02	0.03	0.02	0.02	0.01	0.09	0.02	0.02	0.02
Th	0.08	0.06	0.41	0.63	0.13	0.05	0.10	0.08	0.13	0.17	0.07	0.14	0.07	0.06	0.23	0.10	0.09	0.06
U	0.04	0.05	0.30	0.40	0.03	0.02	0.03	0.02	0.03	0.06	0.02	0.04	0.02	0.01	0.08	0.03	0.02	0.03
Cr/MgO	7.20	70.79	96.56	79.80	23.09	15.70	5.35	16.87	20.06	22.09	21.52	2.48	3.21	14.86	11.99	16.57	95.28	74.87
CaO/Al2O3	0.87	2.22	1.19	1.65	0.61	0.47	0.43	0.45	0.47	0.47	0.45	0.41	0.50	0.55	2.77	0.86	0.69	1.60
V/Cr	2.72	0.10	0.04	0.06	0.73	0.48	2.01	0.37	0.45	0.85	0.54	2.74	0.51	0.69	9.29	0.72	0.11	0.07

(continued on next page)

Table 1 (*continued*)

Sample	CDF9A	CDF9B	N-14	CDF10A	CDF10B	CDF11A	CDF11B	CDF1	CDF2	CDF3A	CDF3B	CDF4	CDF4B	CDF6	CDF7A	CDF7B
Borehole	LAP-31	LAP-31	LAP-31	LAP-31	LAP-31	LAP-31	LAP-31	LAP-04	LAP-04	LAP-04	LAP-04	LAP-04	LAP-04	LAP-04	LAP-04	LAP-04
Depth (m)	-327.12	-327.22	-389.82	-403.95	-404.03	-406.61	-406.69	-270.66	-284.48	-285.55	-285.65	-285.90	-285.95	-287.26	-287.70	-287.76
Rock Unit	1	1	1	2	2	2	1	1	1	2	1	2	2	1	1	1
Lithology	Web	Web	MelGbn	LGbn vein	LGbn vein	LGbn vein	MelGbn	MelGbn	Pxite	LGbn vein	Web	MeGbn	LGbn vein	MelGbn	Web	Web
SiO2	52.95	51.44	51.06	62.51	55.93	56.87	53.99	53.01	53.77	68.38	54.31	50.95	59.07	52.06	52.67	54.07
TiO2	0.23	0.20	0.17	0.09	0.08	0.13	0.18	0.18	0.15	0.35	0.19	0.18	0.34	0.15	0.16	0.16
Al2O3	4.66	5.01	9.79	21.43	16.47	15.35	9.42	10.25	3.94	13.99	3.41	10.68	17.54	11.99	2.29	2.12
Fe2O3	13.27	14.20	9.27	1.20	6.35	6.01	9.87	11.24	12.54	2.62	11.77	13.09	7.16	10.67	10.24	10.15
MnO	0.23	0.35	0.18	0.02	0.13	0.12	0.14	0.20	0.21	0.07	0.22	0.22	0.11	0.13	0.12	0.14
MgO	18.68	21.80	16.83	0.98	9.34	7.78	17.94	14.87	23.18	1.84	21.87	16.53	5.50	13.21	21.65	23.00
CaO	6.22	4.95	9.35	5.52	6.46	9.37	5.27	9.78	4.17	3.58	6.66	6.86	5.82	4.24	7.40	7.16
Na2O	0.20	0.36	1.09	6.18	3.42	2.77	1.31	1.11	0.32	4.77	0.45	1.11	2.91	1.38	0.20	0.27
K2O	0.09	0.11	0.05	0.70	0.33	0.28	0.26	0.14	0.06	1.33	0.02	0.11	1.12	0.17	0.02	0.03
P2O5	0.00	0.01	0.01	0.02	0.01	0.01	0.01	0.00	0.01	0.09	0.00	0.00	0.02	0.02	0.00	0.00
LOI	4.57	1.38	3.26	0.59	0.44	0.48	0.65	0.34	0.91	1.97	1.01	1.38	1.29	4.76	4.70	2.28
Total	101.09	99.81	101.07	99.23	98.95	99.18	99.05	101.10	99.26	98.99	99.91	101.11	100.88	98.77	99.47	99.37
Sc	58.4	52.6	37.7	2.0	21.1	28.6	19.6	39.7	29.9	3.1	29.7	36.6	13.1	27.9	28.7	28.0
V	172.5	151.9	106.8	13.2	76.0	80.5	102.8	160.8	83.9	35.1	94.2	125.6	52.5	85.9	93.6	65.9
Cr	1288.5	1379.5	1232.8	15.0	200.5	203.1	1682.6	966.1	1508.7	16.4	1888.4	501.2	118.4	735.7	2217.0	3065.2
Co	214.1	168.6	62.2	3.3	42.3	36.4	56.9	77.5	69.0	6.3	87.4	79.2	47.5	154.8	94.5	87.2
Zn	127.9	142.8	70.0	34.6	94.5	57.5	87.0	91.4	120.5	26.7	87.9	104.3	62.8	115.1	69.1	70.8
Ga	5.3	4.9	9.8	22.0	14.2	12.7	12.4	8.2	3.7	13.2	4.9	8.2	11.7	9.7	4.8	4.8
Rb	1.9	2.7	0.2	5.6	2.5	4.2	5.9	4.2	3.1	43.2	1.0	2.2	44.7	2.8	1.4	0.9
Sr	14.9	21.7	113.0	729.5	522.6	201.0	116.0	103.8	31.7	211.5	31.5	98.5	173.1	113.3	17.2	27.8
Y	6.1	5.7	6.7	2.6	6.0	7.0	5.4	7.9	2.1	8.2	7.4	6.3	6.5	6.0	9.5	9.6
Zr	20.6	7.2	5.5	21.1	14.6	24.1	14.7	17.8	7.9	128.7	7.9	6.8	131.1	7.4	7.1	9.0
Nb	1.45	0.55	0.47	2.09	1.00	1.77	0.93	0.55	0.34	9.37	0.43	0.43	6.17	0.47	0.32	0.35
Ba	12.61	19.58	27.70	330.42	235.52	106.92	127.99	39.36	10.39	217.45	17.52	41.87	222.82	52.48	1.91	16.50
La	1.52	1.60	1.23	15.03	8.51	4.44	1.69	1.19	0.56	22.35	1.03	1.25	11.71	1.60	1.01	0.98
Ce	3.96	4.00	3.68	22.51	14.20	9.33	4.29	2.77	1.31	38.33	2.58	2.54	18.28	3.44	3.03	2.95
Pr	0.58	0.58	0.52	2.33	1.56	1.24	0.63	0.41	0.18	4.05	0.39	0.36	1.84	0.47	0.52	0.52
Nd	2.32	2.31	2.32	7.07	4.95	4.67	2.43	1.86	0.78	12.67	1.69	1.56	5.63	2.01	2.52	2.51
Sm	0.64	0.60	0.70	1.15	0.97	1.24	0.62	0.60	0.23	2.20	0.55	0.48	1.03	0.61	0.89	0.90
Eu	0.22	0.18	0.29	1.18	0.85	0.37	0.27	0.26	0.09	0.48	0.17	0.23	0.41	0.27	0.25	0.24
Gd	0.65	0.60	0.85	0.87	0.86	1.18	0.67	0.67	0.29	1.94	0.63	0.54	0.96	0.65	1.06	1.03
Tb	0.12	0.11	0.14	0.11	0.13	0.19	0.12	0.13	0.05	0.25	0.12	0.10	0.14	0.12	0.20	0.20
Dy	0.91	0.86	1.04	0.55	0.88	1.21	0.84	0.92	0.40	1.37	0.88	0.75	0.86	0.83	1.35	1.36
Ho	0.20	0.18	0.22	0.09	0.18	0.22	0.17	0.19	0.08	0.24	0.18	0.17	0.17	0.16	0.26	0.26
Er	0.67	0.64	0.65	0.28	0.61	0.69	0.57	0.62	0.30	0.64	0.59	0.55	0.56	0.52	0.86	0.85
Tm	0.11	0.11	0.10	0.04	0.11	0.11	0.09	0.10	0.05	0.09	0.10	0.09	0.09	0.09	0.14	0.14
Yb	0.80	0.80	0.71	0.28	0.83	0.73	0.65	0.68	0.36	0.51	0.68	0.66	0.64	0.57	0.94	0.90
Lu	0.13	0.13	0.11	0.04	0.14	0.11	0.10	0.11	0.06	0.08	0.11	0.11	0.10	0.09	0.15	0.14
Hf	0.42	0.18	0.16	0.52	0.37	0.70	0.39	0.45	0.11	2.89	0.23	0.18	3.13	0.22	0.23	0.25
Ta	0.07	0.02	0.02	0.12	0.07	0.12	0.06	0.04	0.02	0.78	0.03	0.02	0.39	0.03	0.02	0.02
Th	0.10	0.08	0.14	0.74	0.63	1.05	0.35	0.08	0.04	3.65	0.10	0.10	6.18	0.14	0.04	0.07
U	0.09	0.11	0.07	0.73	0.58	0.96	0.14	0.04	0.02	2.02	0.04	0.07	1.71	0.09	0.02	0.03
Cr/MgO	68.97	63.27	73.23	15.30	21.48	26.12	93.78	64.98	65.09	8.91	86.35	30.32	21.51	55.69	102.38	133.29
CaO/Al2O3	1.34	0.99	0.95	0.26	0.39	0.61	0.56	0.95	1.06	0.26	1.95	0.64	0.33	0.35	3.23	3.38
V/Cr	0.13	0.11	0.09	0.88	0.38	0.40	0.06	0.17	0.06	2.13	0.05	0.25	0.44	0.12	0.04	0.02

Key to abbreviations.

Rock units: 1-PGbn (Pigeonite gabbronorite unit), 2-LMGbn (Leuco-mesogabbronorite unit), and 3-PMGbn (Peridotite-melagabbronorite unit).

Lithologies: MeGbn (Mesogabbronorite), LGbn (Leucogabbronorite), Ol Gbn (Olivine gabbronorite), Mgt Gb (Magnetite gabbro), MelGbn (Melagabbronorite), Perid (Peridotite), Web (Websterite), and Pxite (Pyroxenite).

Table 2
Platinum-group element and Au data for Aurora samples.

Sample		P-1	P-2	P-3	P-4	P-5	P-6	P-7	P-8	P-9	P-10	P-11	P-12	P-13	P-14	P-15	P-16	CDF13A
Borehole		LAP-29	LAP-29	LAP-29	LAP-29	LAP-29	LAP-29	LAP-29	LAP-29	LAP-29	LAP-29	LAP-29	LAP-29	LAP-29	LAP-29	LAP-29	LAP-29	LAP-29
Depth from surface (m)		-39.85	-80.15	-144.90	-146.95	-150.10	-194.86	-243.17	-259.77	-266.05	-267.95	-270.23	-275.15	-280.05	-284.86	-390.19	-414.78	-418.17
Rock unit		3	3	2	2	2	2	4	2	2	2	2	2	2	2	1	2	2
Lithology		MeGbn	MeGbn	LGbn	MeGbn	LGbn	Ol Gbnt	MeGbn	LGbn	LGbn	LGbn	LGbn	LGbn	MeGbn	MeGbn	MelGbn	LGbn vein	MeGbn
Ni	ppm	168	197	369	548	154	462	347	92	40	78	338	778	2523	147	241	1718	236
Cu	ppm	374	157	394	121	209	87	246	39	66	223	366	406	3008	114	76	2693	358
Os	ppb	0.06	0.06	2.98	1.00	1.39	0.28	0.19	0.27	0.57	0.44	0.37	1.47	1.18	0.18	0.69	0.96	
Ir	ppb	0.13	0.09	2.37	0.80	1.84	0.37	0.25	0.65	0.66	0.93	1.13	1.52	1.23	0.62	0.72	1.86	
Ru	ppb	0.36	0.17	9.52	6.68	5.37	1.33	0.90	3.17	1.02	2.14	1.92	3.84	3.18	1.23	1.39	2.43	
Rh	ppb	0.12	0.10	9.92	7.00	3.17	0.85	0.65	0.84	1.17	1.00	1.49	2.26	2.98	0.56	0.62	9.23	
Pt	ppb	1.12	2.54	496	86.7	177	78.4	51.9	45.2	30.0	132	304	1812	2676	102	85.8	613	
Pd	ppb	1.68	1.01	639	330	297	143	160	60.4	25.2	103	312	2214	4139	140	68.1	1894	
Au	ppb	0.68	0.81	405	56.6	161	51.9	27.7	17.1	8.88	18.4	298	1342	1417	7.75	4.65	227	
Pt + Pd + Au	ppb	3.48	4.36	1541	473	636	273	240	123	64.1	253	914	5368	8232	249	159	2735	
Pt/Pd		0.67	2.50	0.78	0.26	0.60	0.55	0.32	0.75	1.19	1.28	0.97	0.82	0.65	0.73	1.26	0.32	
Pd/Ir		13.2	11.9	269.7	414.2	161.7	385.3	641.8	92.7	38.0	111.1	276.9	1455	3355	226.8	94.3	1017.3	
Cu/Pd		223,352	154,875	617	368	703	609	1533	639	2618	2171	1171	183	727	814	1123	1421	

Table 2 (*continued*)

Sample	CDF13B	CDF15	P-17	P-18	N-1	N-2	N-3	N-4	N-5	N-6	N-7	N-8	N-9	N-10	N-11	N-12	N-13	CDF08
Borehole	LAP-29	LAP-29	LAP-29	LAP-29	LAP-31	LAP-31	LAP-31	LAP-31	LAP-31	LAP-31	LAP-31	LAP-31	LAP-31	LAP-31	LAP-31	LAP-31	LAP-31	LAP-31
Depth from surface (m)	-418.27	-431.89	-460.31	-479.88	-25.45	-70.23	-80.42	-81.97	-87.50	-100.05	-164.89	-170.31	-174.88	-179.79	-205.05	-254.78	-310.11	-324.66
Rock unit	2	1	1	1	3	2	2	2	2	2	2	2	2	2	4	2	1	1
Lithology	MeGbn	Web	Web	MelGbn	MeGbn	LGbn	LGbn	LGbn	LGbn	LGbn	LGbn	LGbn	Ol Gbn	LGbn	Mgt Gb	MeGbn	MelGbn	Perid
Ni	262	779	652	505	111	76	156	130	429	52	942	56	889	78	325	207	521	1118
Cu	1308	87	101	42	85	35	161	284	409	58	1070	63	291	72	396	56	149	67
Os			1.13	0.66	0.06	0.10	23.3	3.86	1.05	0.22	2.67	0.22	0.29	0.71	0.08	0.17	0.23	1.03
Ir			1.37	0.62	0.07	0.14	31.5	4.89	1.27	0.32	4.66	0.32	0.31	0.73	0.17	0.19	0.35	0.85
Ru			3.97	1.19	0.17	0.50	99.3	16.0	6.56	0.89	12.5	1.19	1.02	3.22	0.39	0.46	0.84	2.08
Rh			1.09	1.04	0.15	0.30	121	11.9	5.54	0.53	6.80	0.77	0.94	1.68	1.36	0.44	0.75	0.47
Pt			14.9	22.1	1.95	3.82	4551	671	101	5.79	1223	41.3	103	137	36.3	88.0	52.7	2.72
Pd			12.7	23.1	1.55	5.42	2962	731	110	10.8	1795	52.0	305	226	34.3	116	105	4.01
Au			5.49	13.4	1.90	5.03	155	181	7.71	5.80	1428	12.5	59.2	16.5	8.86	39.3	27.5	1.32
Pt + Pd + Au			33.1	58.5	5.39	14.3	7668	1583	218	22.4	4446	106	467	380	79.5	243	185	8.05
Pt/Pd			1.18	0.95	1.26	0.70	1.54	0.92	0.92	0.54	0.68	0.79	0.34	0.61	1.06	0.76	0.50	0.68
Pd/Ir			9.3	37.3	22.1	39.2	94.0	149.3	86.0	33.8	385.6	164.8	971.6	310.1	206.7	611.5	295.5	4.7
Cu/Pd			7967	1829	54,877	6454	54	389	3732	5374	596	1220	955	317	11,531	489	1422	16,622

(*continued on next page*)

Table 2 (*continued*)

Sample	CDF9A	CDF9B	N-14	CDF10A	CDF10B	CDF11A	CDF11B	CDF1	CDF2	CDF3A	CDF3B	CDF4	CDF4B	CDF6	CDF7A	CDF7B
Borehole	LAP-31	LAP-31	LAP-31	LAP-31	LAP-31	LAP-31	LAP-31	LAP-04	LAP-04	LAP-04	LAP-04	LAP-04	LAP-04	LAP-04	LAP-04	LAP-04
Depth from surface (m)	-327.12	-327.22	-389.82	-403.95	-404.03	-406.61	-406.69	-270.66	-284.48	-285.55	-285.65	-285.90	-285.95	-287.26	-287.70	-287.76
Rock unit	1	1	1	2	2	2	1	1	1	2	1	2	2	1	1	1
Lithology	Web	Web	MelGbn	LGbn vein	LGbn vein	LGbn vein	MelGbn	MelGbn	Pxite	LGbn vein	Web	MeGbn	LGbn vein	MelGbn	Web	Web
Ni	624	562	414	38	147	169	588	700	806	25	954	428	389	2217	599	683
Cu	68	125	187	5	45	38	44	198	69	20	91	117	725	4616	69	55
Os	0.14	0.14	0.81	0.22	0.26	1.89	1.52	0.67	0.44							
Ir	0.19	0.17	1.12	0.20	0.27	1.71	1.49	0.88	0.69							
Ru	0.38	0.47	3.09	0.40	0.45	2.67	3.50	2.30	1.68							
Rh	0.34	0.69	0.92	0.07	0.06	0.57	1.44	0.55	2.15							
Pt	30.8	21.1	35.1	2.09	15.1	17.0	13.5	41.8	68.4							
Pd	40.8	26.1	56.7	4.90	22.0	14.6	15.8	38.9	101							
Au	3.92	3.40	9.92	0.16	3.25	1.07	0.62	3.32	15.7							
Pt + Pd + Au	75.5	50.6	102	7.16	40.3	32.6	29.9	84.0	185							
Pt/Pd	0.76	0.81	0.62	0.43	0.69	1.16	0.86	1.08	0.68							
Pd/Ir	218.2	149.2	50.8	24.5	81.3	8.5	10.6	44.3	145.3							
Cu/Pd	1669	4779	3291	1015	2064	2627	2791	5086	689							

Key to abbreviations.
Rock units: 1 (Pigeonite gabbronorite unit), 2 (Leuco-mesogabbronorite unit), and 3 (Peridotite-melagabbronorite unit).
Lithologies: MeGbn (Mesogabbronorite), LGbn (Leucogabbronorite), Ol Gbn (Olivine gabbronorite), Mgt Gb (Magnetite gabbro), MelGbn (Melagabbronorite), Perid (Peridotite), Web (Websterite), and Pxite (Pyroxenite).

analyses were IAEA-S-3 (Ag_2S) and NBS-123 (a sulphate standard) international standards, alongside a SUERC laboratory chalcopyrite standard, CP-1. All data are reported in standard per-mille variations from the Vienna Cañon Diablo troilite standard, V-CDT and are given in Table 3.

3. Stratigraphy

Updated logs for LAP29 and LAP31 showing the positions of the samples used in this study and assay profiles for Pt + Pd + Au and for Cr are shown graphically beside the respective log in Fig. 6. The logs for LAP-29 and LAP-31 can be simplified into three major units that are recognisable between the boreholes (Fig. 6). From the base upwards these are: Unit 1, comprising peridotites and melagabbronorites; Unit 2, comprising gabbronorites and leucogabbronorites with rare troctolites and magnetite gabbros; and Unit 3, comprising gabbronorites with cumulus pigeonite (hereafter referred to as pigeonite gabbronorites).

3.1. Logging and petrography of the units

3.1.1. Unit 1 (peridotites and melagabbronorites)

Above the contact with the gneissic basement rocks (which is sometimes marked by a thin zone of fine-grained norite or gabbronorite; see also Manyeruke, 2007) there are 80–100 m of generally medium-grained peridotites and melagabbronorites in LAP-29 and LAP-31. These are classified as orthopyroxenites, websterites or melagabbronorites depending on the proportions of orthopyroxene, clinopyroxene and plagioclase present. Olivine is a minor phase (<10%) in some of the websterites but is absent from the other rock types. Calc-silicate zones (2–6 m thick) are recognised near the base of both boreholes (Fig. 6) and probably represent rafts of dolomitic country rock. Within the medium grained ultramafic rocks there are thin (0.5–10 m thick) layers or veins of medium to coarse-grained gabbronorites and leucogabbronorite that display sharp contacts with the ultramafic rocks and in places carry abundant base metal sulphides (Fig. 5). These veins are observed to cross-cut and produce zones of alteration/recrystallisation in the surrounding rocks and are considered to represent an intrusive part of Unit 2 (see below). The orthopyroxenites are dominated by cumulus orthopyroxene with subsidiary intercumulus clinopyroxene while the websterites display both cumulus ortho- and clinopyroxene. Both rock types contain domains (possibly autoliths) of finer grained pyroxenite and websterite where the crystals show 120° triple junctions, suggestive of recrystallisation and cumulus pyroxenes are sometimes observed crystallized against and around these domains (Fig. 7a and b). Plagioclase content generally increases with height above the floor contact and the feldspar is nearly always intercumulus or interstitial between the pyroxenes. Orthopyroxenes associated with intercumulus plagioclase show evidence of partial corrosion in some samples (Fig. 7c). Patches of granophyre are present between partially corroded pyroxenes in sample P18, collected from ~6 m above the floor contact (Fig. 7d). Granophyre is absent from the other samples and its development would appear to be confined to the base of the unit. Some websterites are altered to serpentine, talc and calcite either pervasively or in narrow veins (Fig. 7e) with evidence for preferential replacement of orthopyroxene over clinopyroxene (Fig. 7f).

3.1.2. Unit 2 (gabbronorites and leucogabbronorites)

These rocks are characterised by coarse-grained cumulus plagioclase. The plagioclase is variably altered and may be 10–40% replaced by spots and patches of very fine-grained mica or clays (Fig. 8a). This alteration is the likely cause of the unusually dark colour displayed by many plagioclase-rich lithologies in core and hand specimen (Fig. 5a). In the lower portion of the unit gabbronorites have cumulus orthopyroxene, but in the upper half pyroxenes are intercumulus or poikilitic and clinopyroxene generally dominates over orthopyroxene. Inverted pigeonite occurs along with orthopyroxene as an intercumulus and interstitial phase from the middle of the unit upwards (Fig. 8b and c). Thin units of olivine gabbronorite or troctolite are present near the middle of the unit in both boreholes. In sample P6 from LAP-29, cumulus olivine is surrounded by successive rims of orthopyroxene and inverted pigeonite (Fig. 8d). Sample N9 from LAP-31 is a troctolite with cumulus olivine and plagioclase and intercumulus clinopyroxene. Thin rims of orthopyroxene are developed on some olivines in N9 but no pigeonite was observed in thin section. Base metal sulphides (aggregates of pyrrhotite, pentlandite and chalcopyrite) are present interstitially between the silicate minerals and along cleavage planes in clinopyroxene in parts of this unit. Medium- and coarse-grained veins of leucogabbronorite that cross-cut ultramafic lithologies in Unit 1 are mineralogically and texturally similar to rocks in Unit 2, but generally lack olivine or pigeonite. Coarse grained base metal sulphides occur within and along the margins of these leucogabbronorite veins.

Zones of coarse-grained to pegmatoidal gabbro ranging from a few centimetres up to 5 m thick are present within Unit 2. These carry ubiquitous cumulus magnetite and sometimes base metal sulphides (pyrrhotite, pyrite and chalcopyrite). Plagioclase and ortho- and clinopyroxene accompany the magnetite and are sometimes strongly altered where they are in contact with base metal sulphides.

3.1.3. Unit 3 (pigeonite gabbronorites)

The upper unit in boreholes LAP29 and LAP31 is dominated by dark, coarse-grained and homogenous gabbronorites that contain abundant inverted pigeonite. Pigeonite in this unit differs texturally from that observed in the unit below. Low-Ca pyroxenes are cumulus and often contain cores of inverted pigeonite surrounded by rims of orthopyroxene (Fig. 8e and f) whereas pigeonite in Unit 2 is always intercumulus or interstitial. Plagioclase may be cumulus or intercumulus depending on the amount of orthopyroxene, while clinopyroxene is generally intercumulus. Xenoliths of calc-silicate up to 2 m thick are present within the pigeonite gabbronorites in LAP-29.

4. Base metal sulphide mineralogy

Base metal sulphides (BMS) occur in different proportions and different textural associations in Units 1, 2 and 4. The available thin sections from Unit 3 contain no visible BMS. The ultramafic rocks of Unit 1 contain small amounts (<0.1%) of interstitial BMS that comprise small (<100 μm diameter) aggregates of pyrrhotite-pentlandite-chalcopyrite (Fig. 9a). The proportion of BMS in the ultramafic rock increases in proximity to cross-cutting felsic veins. Within the felsic veins, the abundance of BMS ranges from <1% to >15%. Massive BMS aggregates with fine stringers of chalcopyrite that have developed along fractures in plagioclase are sometimes developed in the centre and margins of veins (Fig. 9b). Parts of the veins where BMS are locally abundant can produce net-textured sulphides (Figs. 5d and 9c) where pyrrhotite, pentlandite and chalcopyrite enclose rounded clinopyroxene and/or plagioclase. These textures are always restricted to the veins and have not been observed in the ultramafic rocks.

In the gabbronorites and leucogabbronorites of Unit 2, the modal abundance of BMS ranges from <0.5% to approximately 5%. BMS tend to occur as irregular inclusions (comprising pyrrhotite-pentlandite and chalcopyrite) inside clinopyroxene (Fig. 9d) or plagioclase (Fig. 9e). Pentlandite commonly occurs as flames exsolved from pyrrhotite in the upper portions of Unit 2, rather than the coarse granular pentlandite that appears in the veins intruding Unit 1. Chalcopyrite can be found in aggregates with the Fe-Ni sulphide minerals but also as chalcopyrite-dominant zones along cracks or in alteration patches within both plagioclase and pyroxene (Fig. 9e). Some magnetite-rich

Table 3
Sulphur isotope data for La Pucella and Nonnenwerth.

Sample	Lithology	$\delta^{34}S$ (‰ VCDT)	Source
LAP29	Granite	−1.5	a
LAP26	Granite	0.1	a
LAP31	Granite	0.5	a
LAP47	Granite	1.3	a
LAP47	Granite	−0.9	a
LAP47	Granite	0.2	a
LAP52	Granite	0.8	a
MOX9	Recrystallised gabbronorite	1.33	b
MOX10	Recrystallised gabbronorite	1.22	b
MOX14	Melagabbronorite	1.87	b
MOX27	Anorthosite	1.33	b
MOX29	Gabbro	0.73	b
MOX33	Norite	1.22	b
MOX36	Altered gabbronorite	5.24	b
LAP 29-P3	Leucogabbronorite	−0.8	c
LAP 29-P5	Leucogabbronorite	0.6	c
LAP 29-P11	Leucogabbronorite	−0.2	c
LAP 29-P13	Mesogabbronorite	0.1	c
LAP 29-P16	Mesogabbronorite	0.3	c
LAP 31-N3	Leucogabbronorite	−0.1	c
LAP 31-N7	Leucogabbronorite	1.1	c

Data sources: (a) Holwell et al., 2007; (b) Manyeruke (2007); and (c) this work.
3 dimensional block diagram showing the position of the Aurora mineralisation and the potential for it extending north into the Waterberg deposit and south into a prospective but unexplored target zone in the Upper Main Zone.

gabbros are also rich in BMS. Observations suggest that these aggregates are dominated by pyrrhotite and chalcopyrite, with little pentlandite. Pyrite is sometimes developed along the contact between the Fe-Cu sulphides and magnetite (Fig. 9f), possibly in response to Fe exchange between the sulphide and the spinel (c.f. Naldrett and Lehmann, 1988).

5. Bulk compositions

5.1. Major and trace elements

The peridotites and melagabbronorites of Unit 1 are enriched in Mg (>10% MgO) and Cr (600-2000 ppm) with Cr/MgO ratios between 70 and 125 (Table 1); comparable to Platreef or Upper Critical Zone values (Seabrook et al., 2005; Kinnaird et al., 2005; McDonald and Holwell, 2011; Kinnaird and Nex, 2015). Mantle normalized lithophile element profiles for the peridotites and melagabbronorites of Unit 1 (Fig. 10a–b) show generally flat profiles with most lithophile element concentrations at ~0.8–2× mantle values. The profiles display consistent negative Th, Nb-Ta, and Ti anomalies. Zr and Hf are variably depleted and Sr is variably enriched or depleted relative to the other lithophile elements. Despite their mineralogical similarities, the ultramafic rocks lack the light rare earth element (LREE) enrichment and the broad U-shaped pattern with middle rare earth element (MREE) depletion and slight heavy rare earth element (HREE) enrichment found in many Platreef pyroxenites (Fig. 10h). The granophyre-bearing melagabbronorite (P18) at the base of LAP-29 is enriched in all trace elements relative to the other ultramafic samples from this borehole (Fig. 10a). The coarse-grained felsic veins sampled in LAP-31 and LAP-04 are also strongly enriched in large ion lithophile (LIL) elements and LREE compared with the ultramafic rocks (compare open versus filled symbols in Fig. 10b and c).

The gabbronorites and leucogabbronorite veins of Unit 2 are characterised by higher Al, Sr and low Cr concentrations; with Cr/MgO ratios between 2 and 40 (Table 1); typical of many Main Zone rocks (Seabrook et al., 2005). The mantle normalized profile shapes in LAP-29 and LAP-31 are very similar (Fig. 10d and e) and show prominent positive Sr and Eu anomalies, with negative Th, Nb-Ta and Ti anomalies

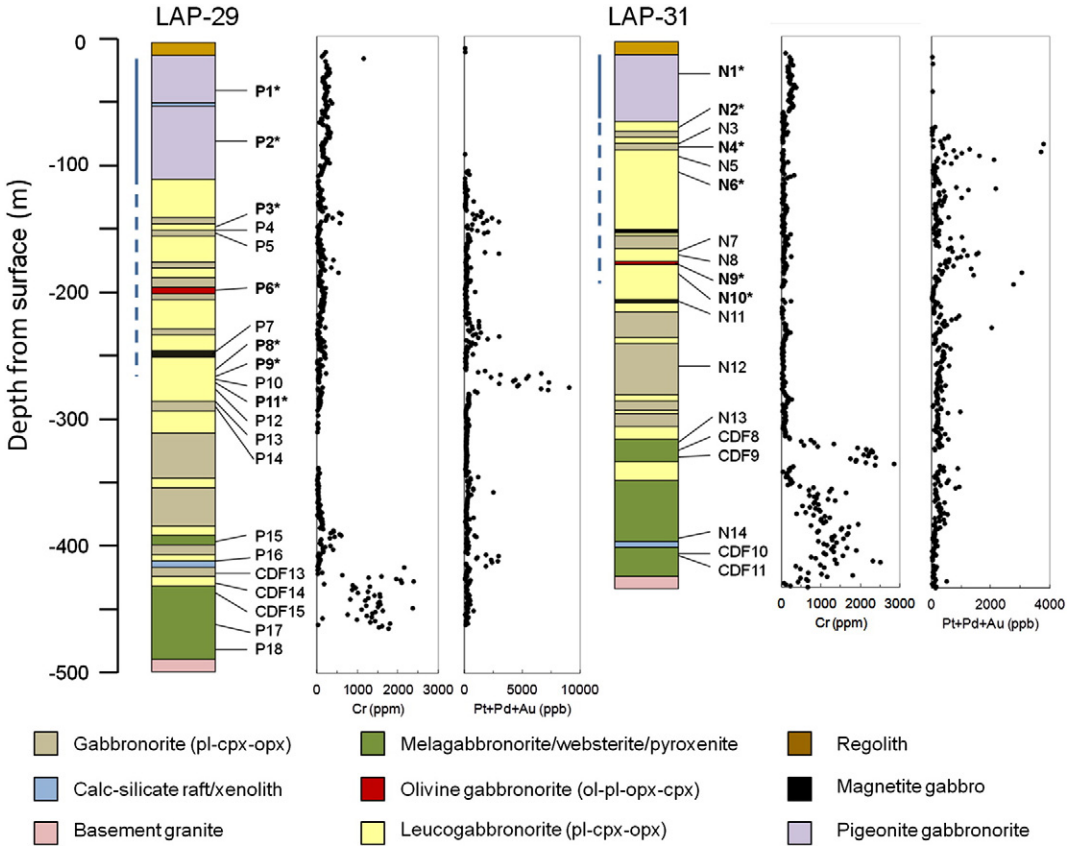

Fig. 6. Lithological logs for LAP-29 and LAP-31 with Cr and (Pt + Pd + Au) grades determined by XRF and Pb fire assay respectively. Sample numbers shown in bold with asterisks indicate that the sample contains inverted pigeonite. The distribution of pigeonite is also shown graphically with a blue vertical line. Cumulus pigeonite is indicated with a solid blue line and intercumulus pigeonite with a dashed line.

superimposed on a slightly LREE-enriched profile. Olivine gabbronorites and troctolites found within the unit display similar profiles to the olivine-free felsic rocks (compare Fig. 10d–f). Pigeonite gabbronorites from Unit 3 have similar pattern shapes to the gabbronorites and leucogabbronorites of Unit 2 but with smaller Sr and Eu anomalies and greater absolute concentrations of lithophile elements (Fig. 10g).

Magnetite-rich gabbros (represented by samples P7 and N11) are strongly enriched in Fe, Ti, P and V compared with all of the other rocks. The normalized lithophile element profiles are also very different. Ba and Th are depleted relative to the LREE, Sr and Ti anomalies are negative and positive respectively. La and Ce are depleted in comparison to the other LREE and the HREE are only slightly depleted relative to LREE (Fig. 10f). gabbronorites.

The mantle normalised profiles of all of the Aurora rocks, even the pyroxenites and websterites of Unit 1, are significantly different from those measured from the geographically closest Platreef rocks on the farm Overysel (Fig. 10h). Negative Nb-Ta anomalies are more pronounced and enrichments in Ba, U and LREE are stronger in the Platreef rocks compared with Aurora.

5.2. Platinum-group elements and gold

The most striking difference between the mineralisation at Aurora and other major Bushveld PGE deposits is that PGE and Au mineralisation at Aurora is hosted predominantly in felsic rather than in ultramafic rocks, in contrast to the Platreef, the Merensky Reef or the UG2 chromitite (Fig. 6). On a metre-scale, PGE + Au grade is anti-correlated with both Cr and MgO; grade maxima invariably correspond with Cr minima (Fig. 6), and relate to veins or layers of gabbronorites and leucogabbronorite within the peridotite-melagabbronorites of

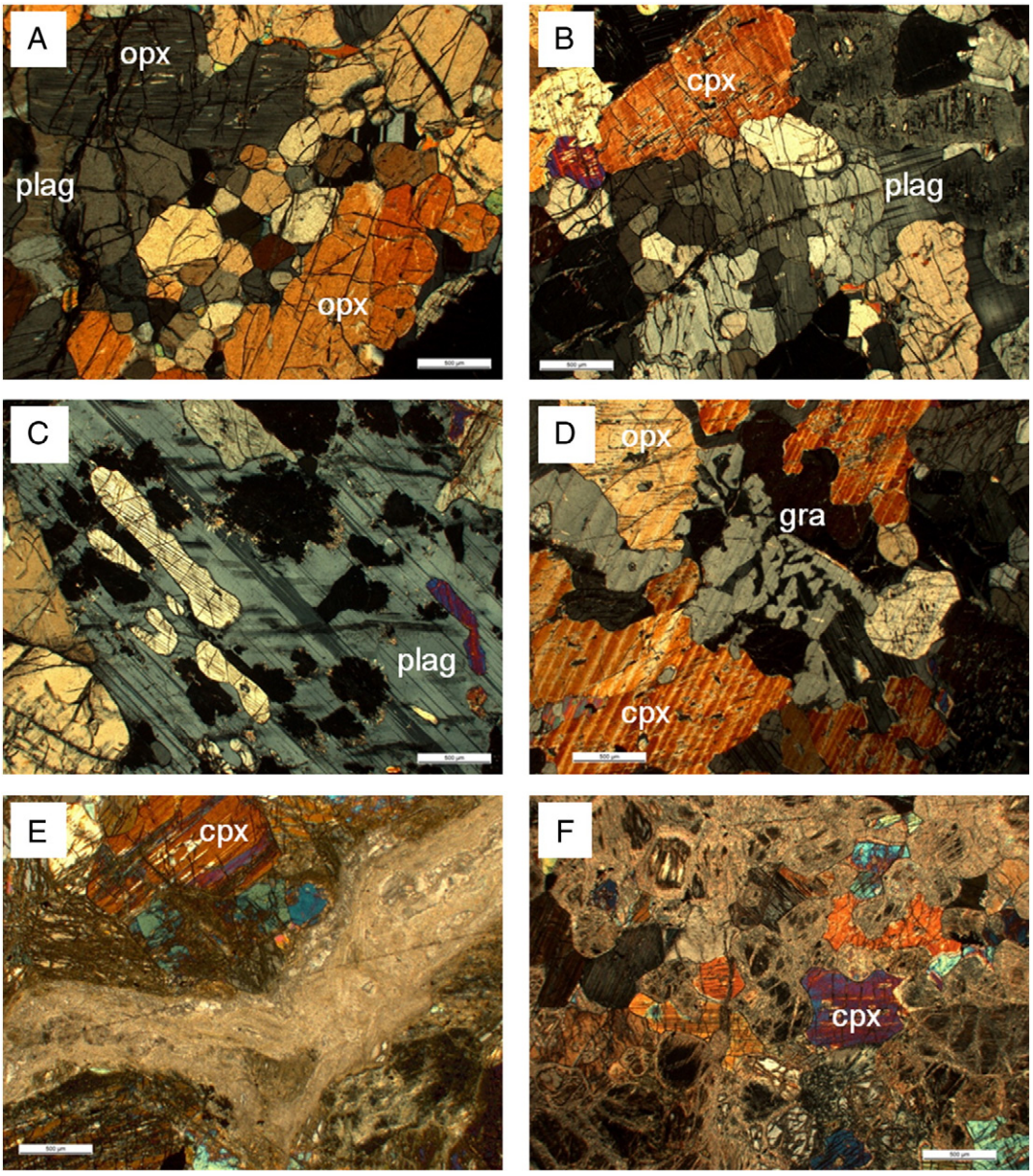

Fig. 7. Examples of websterites and melagabbronorites. (A) CDF8; coarse grained orthopyroxene surrounding recrystallised fine grained websterite. (B) P17; cumulus orthopyroxene surrounding fine-grained recrystallised orthopyroxenite. (C) CDF15; intercumulus plagioclase containing resorbed orthopyroxene. (D P18; granophyre infiltration between partially resorbed orthopyroxenes. (E) CDF2; talc-carbonate vein with sulphides (opaque) in websterite. (F) P11; preferential replacement of orthopyroxene in altered websterite. Scale bar = 500 μm in all diagrams.

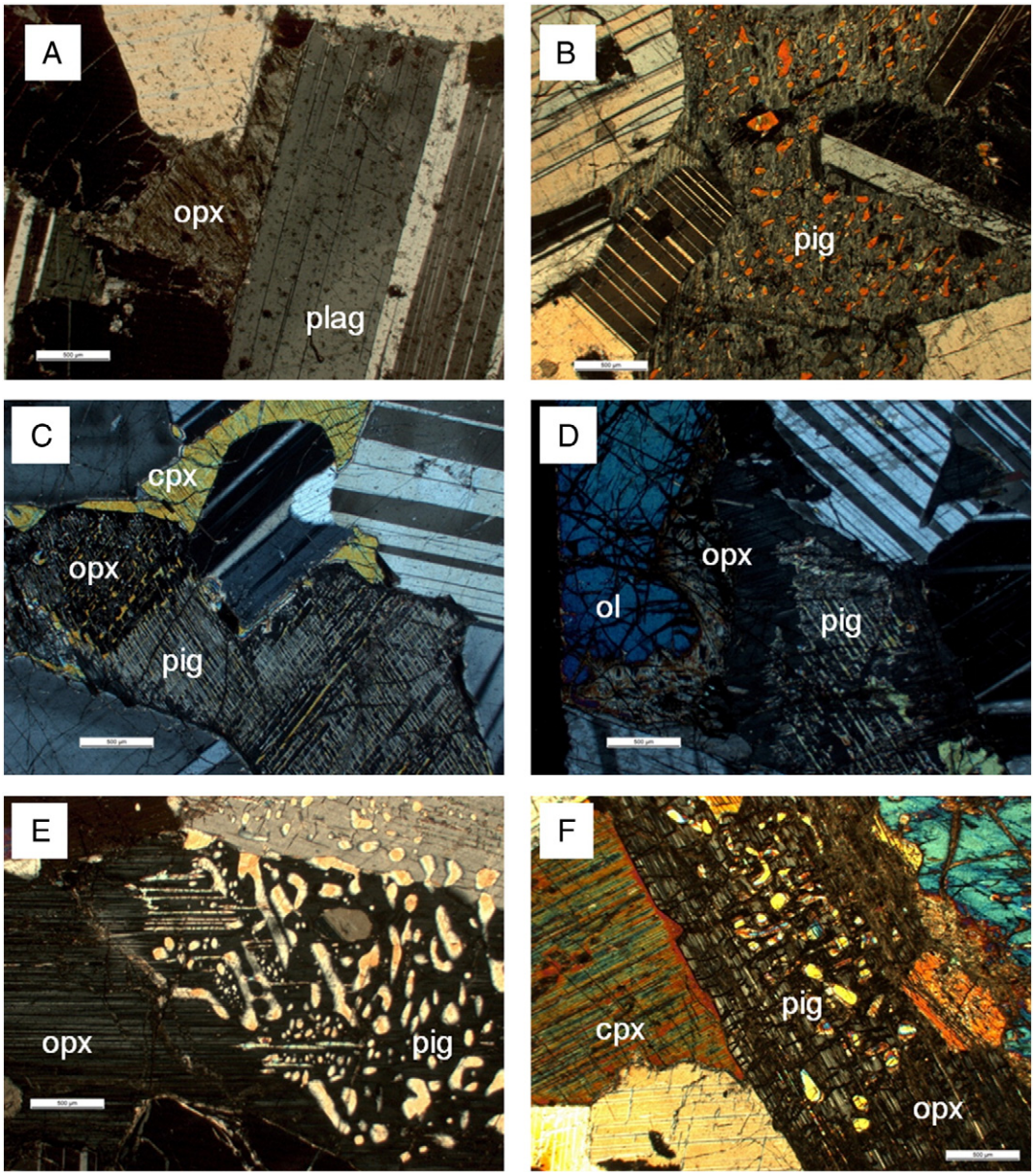

Fig. 8. Occurrences of inverted pigeonite in lithological Units 2 and 3. (A) N6; altered cumulus plagioclase with intercumulus orthopyroxene. (B) P11; intercumulus inverted pigeonite with cumulus plagioclase. (C) P6; olivine mantled by orthopyroxene and pigeonite. (D) P6; intercumulus orthopyroxene and inverted pigeonite. (E) N1; cumulus orthopyroxene with an inverted pigeonite core. (F) P2; cumulus orthopyroxene with an inverted pigeonite core. Scale bar = 500 μm in all diagrams.

Unit 1. Using a simple plot of Pt + Pd + Au versus Cr, the Aurora data cluster along the x and y axes, with any appreciable grade (considered to be >1000 ppb combined Pt + Pd + Au) restricted to rocks with significantly <300 ppm Cr (Fig. 11a). This contrasts markedly with the relationship found in the Platreef (Fig. 11b) where data from the least contaminated Platreef pyroxenites show a very broad and consistent relationship between PGE grade and Cr concentrations (Fig. 11b). The Aurora distribution is also different from that found in the Lower Mafic Unit (LMF) and Mottled Anorthosite Unit (MANO) that form the Grasvally Norite-Pyroxenite-Anorthosite (GNPA) member on the farms Grasvally and Rooipoort (Smith et al., 2014; Fig. 11c). The BMS mineralisation at Moorddrift (Fig. 1) is similarly restricted to Cr-poor rocks, albeit without an accompanying suite of Cr-rich but PGE-poor ultramafic rocks (Fig. 11c).

Chondrite normalized plots for PGE and Au in Fig. 12a and b show that the peridotites and melagabbronorites of Unit 1 are characterised by shallow profiles across the Ir-group PGE (IPGE) and Rh, with elevated Pt, Pd and Au (Pd/Ir 4.7–218). Total PGE concentrations in the ultramafic rocks vary between 7 and 185 ppb, with the highest concentrations found towards the top of the unit or close to any intrusive veins (Table 2), probably reflecting the abundance of fine grained disseminated BMS observed. The ultramafic rocks are consistently depleted in IPGE and show different profile shapes to those that are found in the Platreef. An intrusive gabbronorite (P16) within Unit 1 carries significantly higher grade and with a more strongly fractionated PGE profile compared with the pyroxenites and websterites (Fig. 12b).

The gabbronorites and leucogabbronorites of Unit 2 have strongly fractionated PGE patterns (Pd/Ir 24–3355; Table 2). The profiles from Os to Rh tend to be flat or moderately fractionated at <0.01 × chondrite and in the most enriched samples there is a prominent slope change between Rh and Pt and very strong enrichment in Pt and Pd with variable

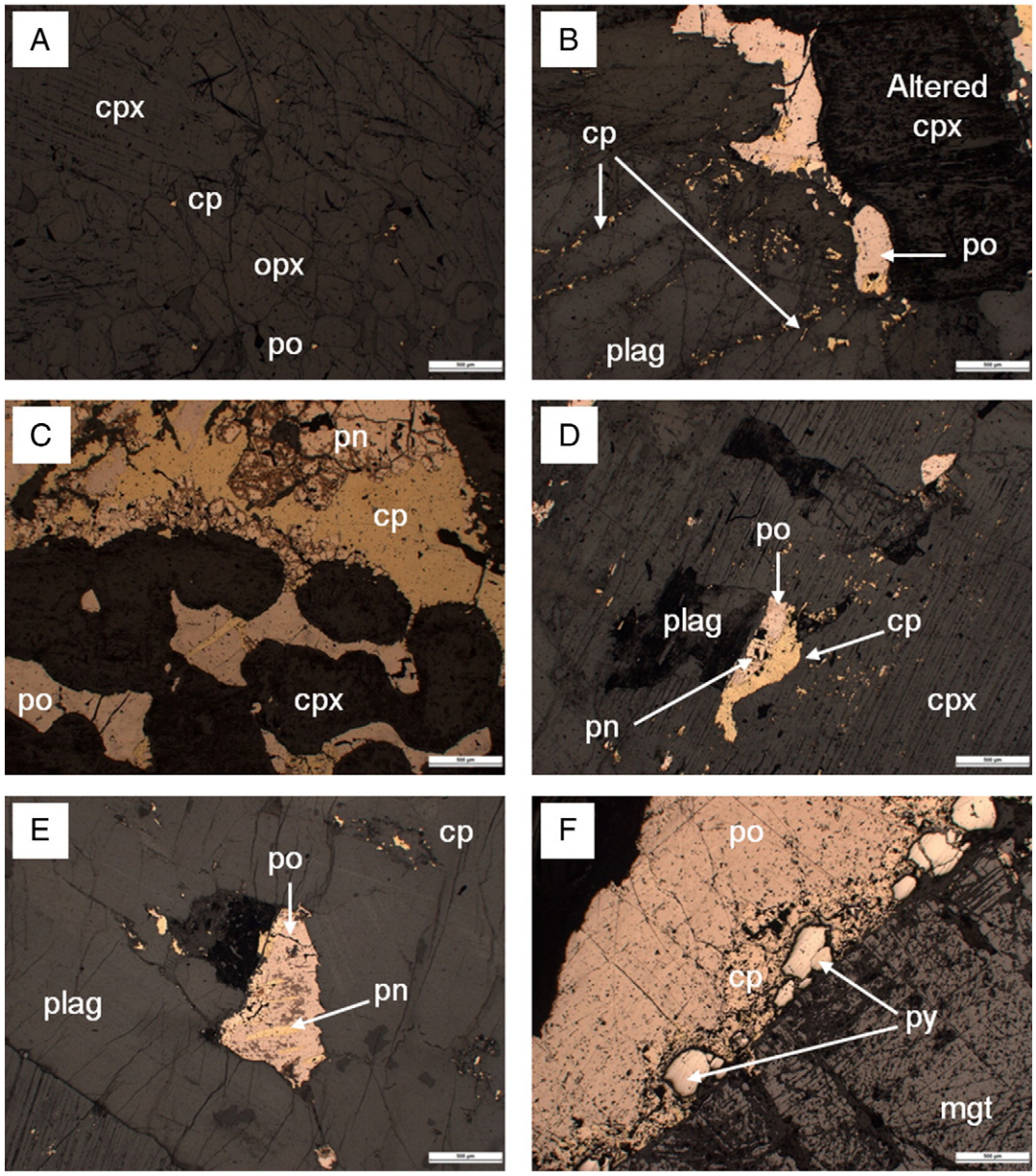

Fig. 9. Reflected light images of sulphide and oxide textures. (A) CDF2 (LAP-04); fine grained interstitial sulphides in Unit 1 websterite. (B) CDF5 (LAP-04); coarse sulphides in leucocratic vein with plagioclase and altered clinopyroxene. Note stringers of chalcopyrite in plagioclase. (C) CDF6 (LAP-04); net-textured sulphides with irregular clinopyroxene (now altered to chlorite and talc). (D) P3; sulphide-plagioclase inclusion in fresh clinopyroxene. (E) P3; pyrrhotite with exsolved pentlandite in plagioclase. Chalcopyrite is associated with cracks and alteration pockets in the feldspar. (F) P4A; Pyrrhotite-chalcopyrite with pyrite developed in contact with magnetite. Abbreviations: pyrrhotite (po), pentlandite (pn), chalcopyrite (cp), pyrite (py), magnetite (mgt), plagioclase (plag) and clinopyroxene (cpx). Scale bar = 500 μm in all diagrams.

enrichment in Au. These profiles are more strongly fractionated than the Platreef (reflecting IPGE depletion) and many samples display enrichment in Au; another feature not commonly associated with Platreef rocks (Fig. 12c and d). Olivine-bearing units within the gabbronoritesleucogabbronorite unit are also characterised by strongly fractionated patterns controlled by IPGE depletion and enrichment in Pd and Au (Fig. 11f). The magnetite gabbros within Unit 2 contain lower absolute PGE concentrations than the troctolites, olivine gabbronorites and leucogabbronorites of Unit 2. IPGE concentrations are very low (<1 ppb) and the profile shapes are strongly fractionated (Pd/Ir 206–641). All samples from the pigeonite gabbronorites (Unit 3) carry very low total concentrations of PGE (<5 ppb) and display smoothly sloping patterns (Fig. 12e).

Fig. 13a and b illustrates the variation in Cu/Pd ratio with depth in LAP-29 and LAP-31. Cu/Pd ratios in Unit 1 are >1000 and generally higher than in Unit 2. Leucogabbronorite veins in Unit 1 also have consistently lower Cu/Pd than surrounding ultramafic rocks and there may be a trend towards lower Cu/Pd moving upwards through Unit 2. Cu/Pd ratios of Unit 3 rocks are consistently high, >50,000, indicating strong depletion in Pd relative to Cu compared to the B1 (Cu/Pd average 4021; Barnes et al., 2010) or B3 (Cu/Pd average 1106; Barnes et al., 2010) magmas assumed to be parental to the Bushveld Complex. On a Cu/Pd versus Pd plot (Fig. 13c) the pigeonite gabbronorites of Unit 3 lie close to the expected trend for a model B3 Main Zone-type magma that has been depleted of chalcophile elements at a high R factor. Samples from Units 1 and 2 have lower Cu/Pd and lie to the right of the Main

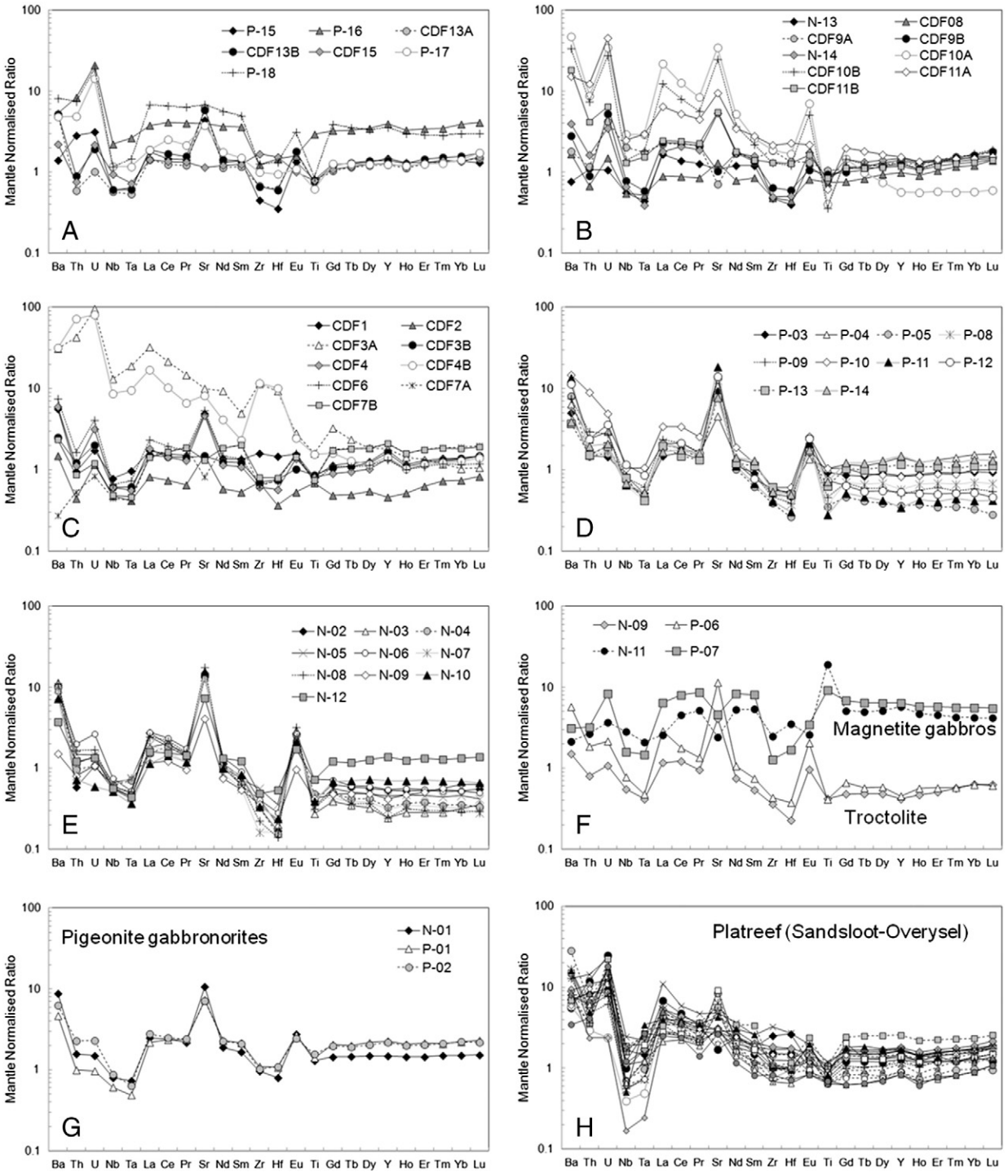

Fig. 10. Mantle normalized spidergrams for different rock units. Normalization values from McDonough and Sun (1995). (A) Peridotite-melagabbronorites in LAP29; (B) Peridotite-melagabbronorites and intrusive veins in LAP31; (C) Peridotite-melagabbronorites and intrusive veins in LAP04; (D) Leucogabbronorites and-gabbronorites in LAP29; (E) Leucogabbronorites and gabbronorites in LAP31; (F) Troctolites and magnetite gabbronorites; (G) Pigeonite gabbronorites; (H) Platreef pyroxenites from Sandsloot and Overysel (Platreef data from McDonald and Holwell, 2011).

Zone magma composition and may be modelled as mixtures of silicate and sulphides generated at R factors of 10^4 to 10^5.

6. Mineral chemistry

Major element data for pyroxenes and plagioclase in LAP-29 and LAP-31 and trace element data for pyroxenes and plagioclase in LAP-29 determined by LA-ICP-MS are given in Supplementary Tables S4–S6 and chemical trends are presented graphically in Fig. 14. Low-Ca pyroxenes in Unit 1 are Mg-rich (Mg# 70–79); similar to values found in the Platreef (e.g. Buchanan and Rouse, 1984; McDonald et al., 2005; Manyeruke et al., 2005; Yudovskaya et al., 2011; Hutchinson et al., 2015) and the Troctolite Unit recognised in the middle of the Main Zone (der Merwe M.J., 1978; Ashwal et al., 2005). Mg# values of low-Ca pyroxene decline upwards in LAP-29 but the same trend is not obvious in LAP-31 (Fig. 14). Concentrations of Cr in pyroxene mirror Mg# but Mn shows the opposite trend. Cr concentrations in low-Ca pyroxene of Unit 1 at Aurora are

significantly lower (1200–2000 ppm) than in the Platreef (3500–4000 ppm) whereas Mn is higher (2900–3200 ppm) than the Platreef (~1900 ppm; Roelofse and Ashwal, 2012; Tanner et al., 2014). Concentrations of Cr and Mn are similar to those found in low-Ca pyroxene from the Troctolite Unit (Ashwal et al., 2005; Tanner et al., 2014).

In the gabbronoritesleucogabbronorites of Unit 2, Mg# values in low-Ca pyroxene are generally lower (Mg# 60–75) and are likely to be strongly affected by trapped liquid shift effects in samples with high modal plagioclase (c.f. Meurer and Boudreau, 1998; Cawthorn, 2002). There is evidence for a progressive reversal towards higher Mg# between Units 2 and 3 in LAP-31 but this is less clear in LAP-29 due to the smaller number of samples that cover this interval. Olivine-rich portions of unit 2 in both boreholes show increased Mg# in low-Ca pyroxenes relative to samples above and below (Fig. 14). Cr concentrations in low-Ca pyroxenes from Unit 2 and Unit 3 are 3–5 times lower than Unit 1, whereas Mn shows the opposite trend and is 1.2–2× higher in Units 2 and 3 compared with Unit 1. Low-Ca pyroxenes in magnetite gabbros are systematically more Fe-rich (Mg# 56) than the other lithologies.

In all units, the Mg# value for clinopyroxene mirrors that of orthopyroxene but with a positive offset that varies from +4 to +10 Mg# units (not shown; see Supplementary Tables S5 and S6). The offset is greatest in the most plagioclase-rich units and has been noted as a widespread feature in the northern limb Main Zone by Ashwal et al. (2005), Roelofse and Ashwal (2012) and Tanner et al. (2014).

Plagioclase from closest to the floor contact in Unit 1 displays large variations in composition (An_{36-67}). The most sodic compositions are from plagioclase that is spatially associated with granophyre (Fig. 7c). At the top of Unit 1, >100 m above the floor contact, plagioclase compositions fall into a more restricted range (An_{67-75}). Concentrations of Ba and Sr in plagioclase in Unit 1 are <300 ppm and <90 ppm respectively (Fig. 14).

In Unit 2, plagioclase displays a narrow range of compositions (An_{67-75}) except for the upper 40 m of the sequence in LAP-31 where there is a trend towards more sodic compositions (An_{60-66}) that continues into Unit 3 (Fig. 14). Sr concentrations do not significantly change across this interval but Ba concentrations increase from ~60 ppm to ~95 ppm in LAP-29 (Fig. 14). There is no difference in major or trace element compositions of plagioclase in olivine-bearing versus olivine-free portions of Unit 2. However, magnetite-rich gabbros in both boreholes are characterised by consistently more sodic plagioclase (An_{57-58} in LAP-31 and An_{38-40} in LAP-29) compared with Unit 2 samples immediately above and below.

7. Sulphur isotopes

Conventional sulphur isotope analyses were carried out on 5 bulk samples from LAP-29 and 2 samples from LAP-31. All samples bar one were selected from Unit 2 and the other (P16) was taken from a Cr-poor cross-cutting gabbronorite within Unit 1. The results are summarised in Table 3 and graphically in Fig. 15 alongside data from the geographically closest Platreef (Overysel-Sandsloot), and potentially analogous sulphide mineralisation in the plagioclase-rich MANO portion of the GNPA member on the farm Rooipoort, and from the Main Zone on the farm Moorddrift.

The $\delta^{34}S$ values for Unit 2 at La Pucella cover a narrow range from −0.8 to +1.1‰ that is indistinguishable from the estimated local mantle value of 1.0‰ (mean of 44 determinations: Westerlund et al., 2004). Fig. 15a illustrates the overlap with previous data for sulphides in basement granites at La Pucella (Holwell et al., 2007) and for mineralized leucogabbronorites on Nonnenwerth (Manyeruke, 2007). The mode at Aurora lies between 0 and +1‰, which is lighter than that of primary Platreef (Holwell et al., 2007; Fig. 15b). Mineralized rocks from Rooipoort and Moorddrift carry S that is consistently isotopically heavier than Aurora (Fig. 15c); a feature already highlighted by Holwell et al. (2013).

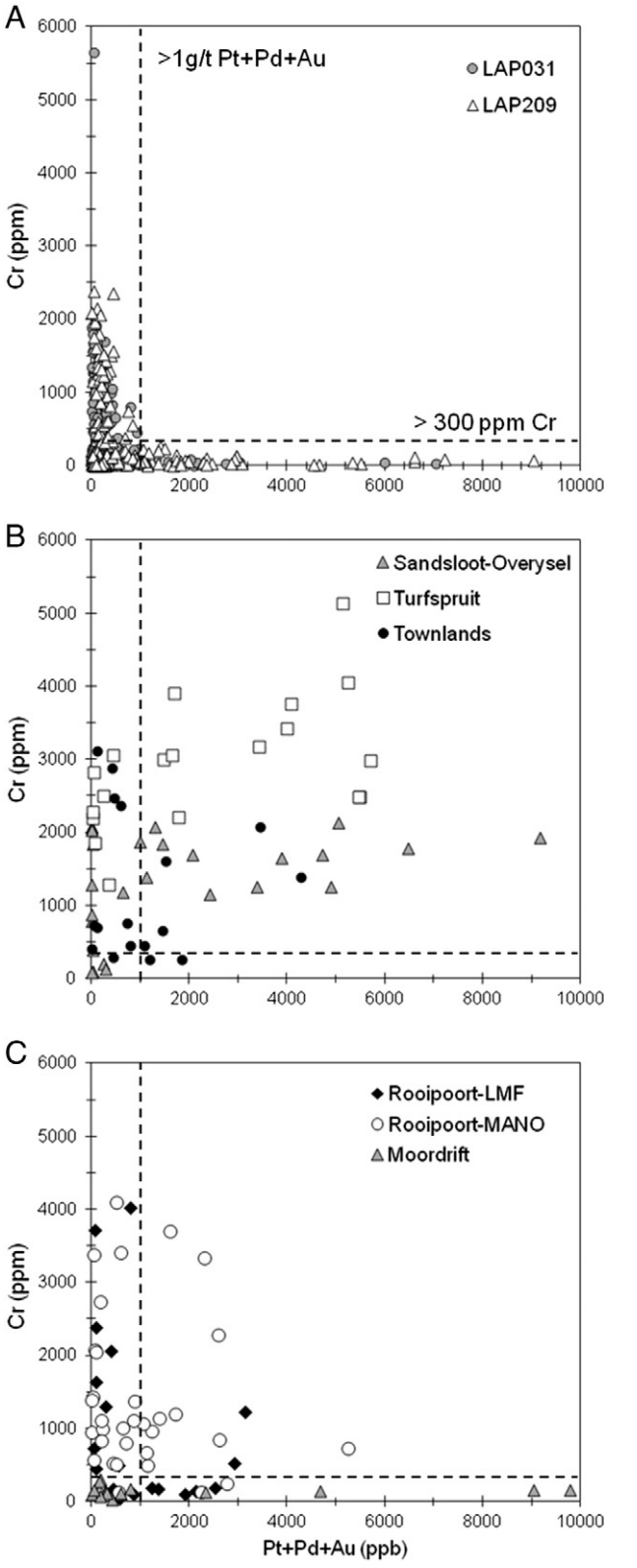

Fig. 11. PGE grade versus Cr concentrations. (A) La Pucella (this work); (B) Platreef at Sandsloot (Holwell, 2006; McDonald et al., 2005); Turfspruit (Smart, 2013) and Townlands (Manyeruke et al., 2005); (C) Lower Mafic Unit and Mottled Anorthosite Unit at Rooipoort (Maier et al., 2008; Smith et al., 2014) and Moordrift (Maier and Barnes, 2010).

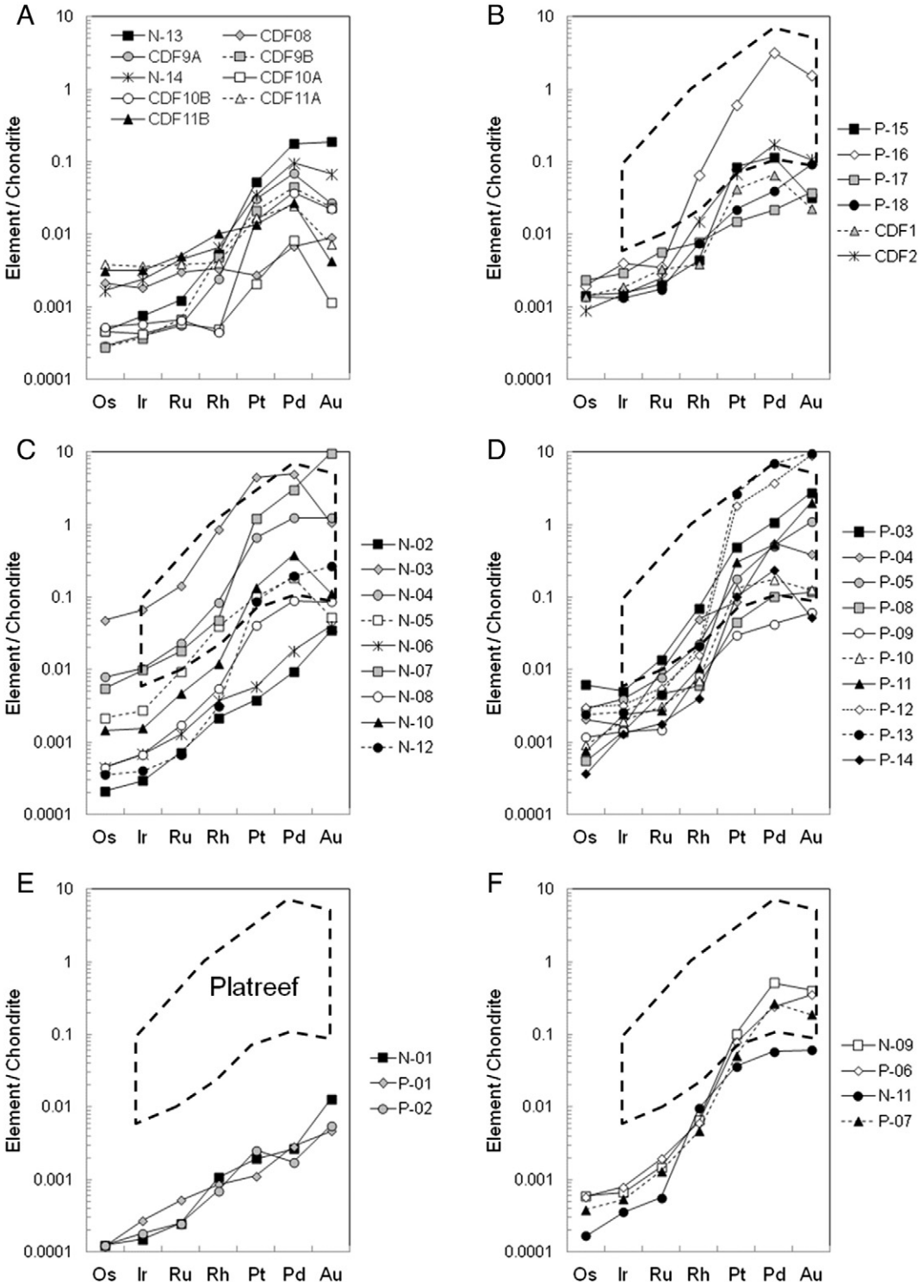

Fig. 12. Chondrite normalized PGE plots. (A) Peridotites and melagabbronorites from LAP-31; (B) Peridotites and melagabbronorites from LAP-29 plus intrusive gabbronorite P16. (C) Leucogabbronorites and -gabbronorites from LAP-31; (D) Leucogabbronirites and gabbronorites from LAP-29, (E) Pigeonite gabbronorites; and (F) Troctolites and magnetite gabbros. Dashed field for Platreef pyroxenites from Sandsloot and Overysel (Holwell and McDonald, 2006).

8. Discussion

Given the global significance of the northern limb of the Bushveld Complex in terms of Ni-Cu-PGE resources it is critical to determine whether the Aurora mineralisation relates to a contact-type Platreef deposit as envisaged by Maier et al. (2008), or to a Main Zone-style deposit as envisaged by Maier and Barnes (2010), or whether it is something else entirely. As such, the most critical information by which to test these models are the ability to correlate the host stratigraphy and the geochemical and mineralogical characteristics of the mineralisation itself. Any explanation for the magmatic stratigraphy and the development of mineralisation at Aurora must account for the following key observations:

(i) the mixture of leucocratic and ultramafic rocks within the stratigraphy;

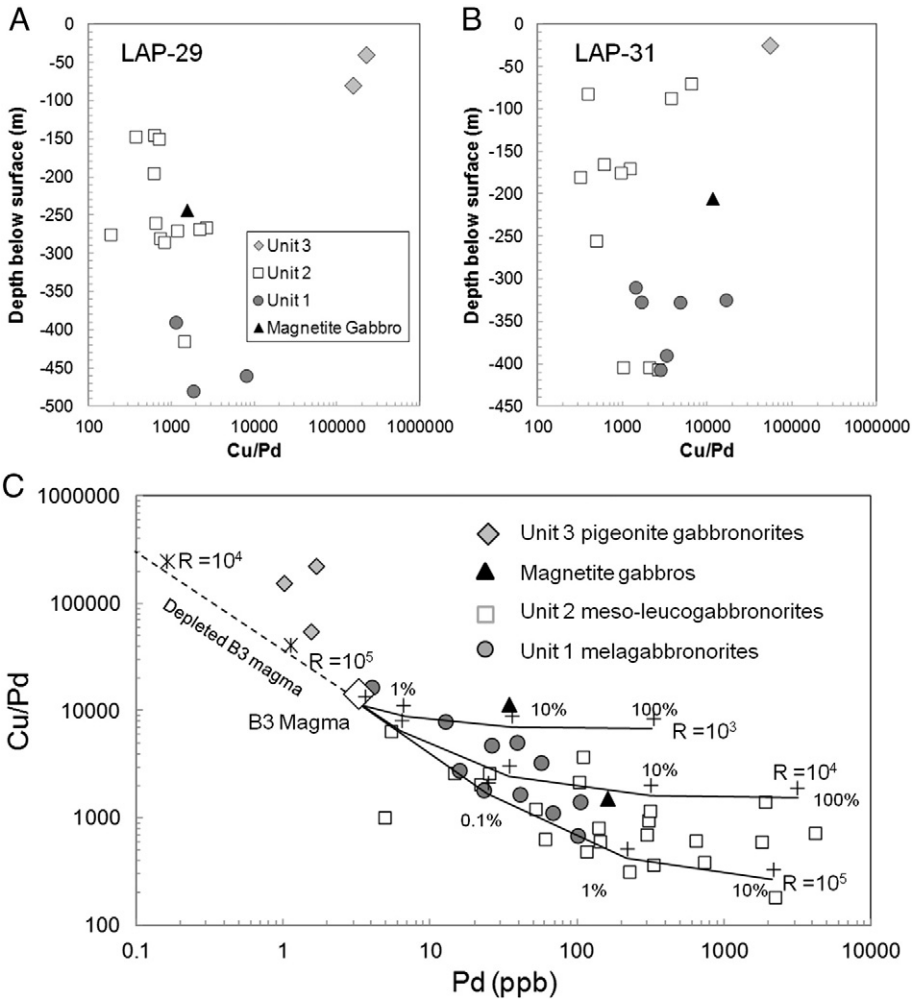

Fig. 13. (A) Cu/Pd with depth for LAP-29. (B) Cu/Pd with depth for LAP-31. (C) Cu/Pd versus Pd for Aurora samples. Average B3 (Main Zone) magma composition is from Barnes et al. (2010). D values for Cu and Pd are assumed to be 1470 and 190,000 respectively (Mungall and Brenan, 2014). Model lines represent mixtures between sulphides and liquid equilibrated at different R factors. The depleted model line shows the position of B3 magma that has been completely equilibrated with sulphide at R factors of 10^4 and 10^5.

(ii) the presence of pigeonite (inverted to orthopyroxene) through the upper part of Unit 2, becoming abundant in the overlying pigeonite gabbronorites of Unit 3;
(iii) major and trace element chemistries of pyroxenes and plagioclase that differ from the Platreef or the Critical Zone;
(iv) the strong correlation between Cu-Ni-PGE-rich BMS and plagioclase-rich rocks that is opposite to the Platreef and stratiform PGE-rich layers in the Critical Zone;
(v) strong fractionation between the IPGE and Pt, Pd and Au indicating the involvement of a different or more evolved magma than was involved in the generation of the Platreef and the PGE deposits of the Critical Zone
(vi) the presence of magnetite-rich gabbros with Fe-rich pyroxene and Na-rich plagioclase within Unit 2.

With these observations noted, we tackle a series of questions that are intended to help establish the likely position of the Aurora mineralisation within the stratigraphy of the northern limb and any links with other known PGE mineralisation.

8.1. Is Aurora a northern extension of the Platreef?

This study has shown that PGE mineralization on La Pucella is hosted by leucocratic rather than ultramafic rocks. The same holds for Nonnenwerth and for Kransplaats (Harmer et al., 2004; McDonald and Harmer, 2010) and this seems to be a general feature of the Aurora Project. Manyeruke (2007) and Maier et al. (2008) chose to divide the package of rocks on Nonnenwerth into a lower "Platreef" and an upper "Main Zone", separated by prominent horizons/xenoliths of dolomite, and with grade restricted to the lower "Platreef" portion. Despite this classification, in both of the boreholes studied by Manyeruke (2007), significant grade is restricted to plagioclase-rich gabbronorites. Also, the chilling/erosion and the abrupt changes in bulk major element chemistry and in mineral chemistry that occur at the boundary between the Platreef (sensu stricto) and the Main Zone (e.g. Gain and Mostert, 1982; Harris and Chaumba, 2001; McDonald et al., 2005; Kinnaird et al., 2005; Holwell et al., 2005; Holwell and Jordaan, 2006) are not present. The most mineralized rocks analysed in this study and in Manyeruke (2007) all have Cr/MgO ratios <60 (more commonly <25), suggestive of a Main Zone origin (Seabrook et al., 2005; McDonald and Holwell, 2011).

The Aurora rocks that most resemble the Platreef (sensu-stricto) are the peridotites and-melagabbronorites of Unit 1. While these rocks do have Cr/MgO ratios >80 and are mineralogically similar to the Platreef and the Critical Zone, they are not strongly mineralized apart from small amounts of disseminated BMS close to intrusive veins (Fig. 5). Unit 1 rocks differ from typical Platreef in terms of both lithophile element and PGE geochemistry (Figs. 10 and 12) and the Aurora pyroxenes contain significantly less Cr, and more Mn, than the Platreef pyroxenes (Supplementary Tables S5 and S6). While Unit 1 cannot be a direct equivalent to the Platreef, it nevertheless must represent an intrusion of a relatively Cr-rich mafic magma into dolomitic rocks (partially preserved as xenoliths and rafts) close to the regional unconformity with

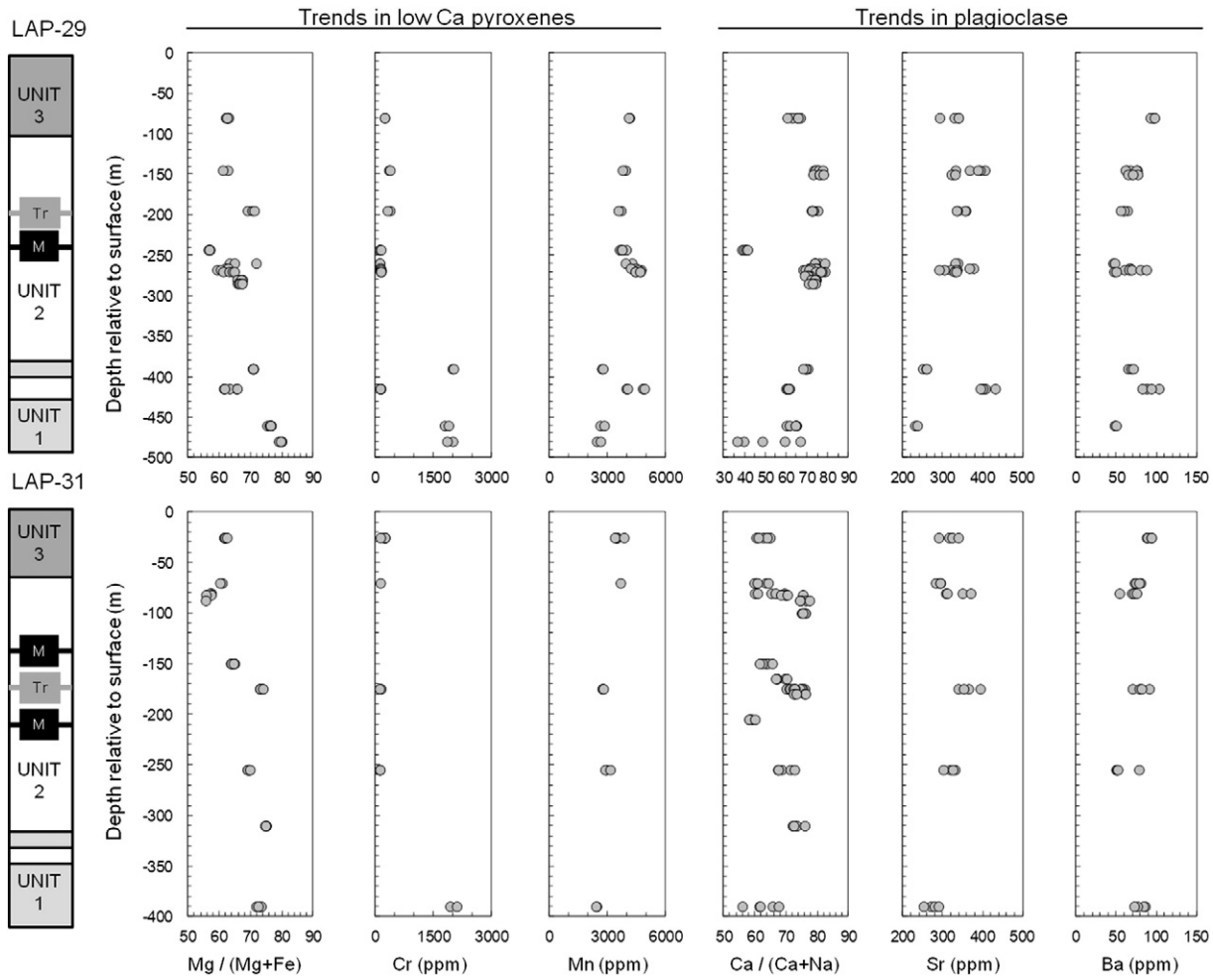

Fig. 14. Major and trace elements in low-Ca pyroxene and plagioclase for LAP-29 and LAP-31. Data from Supplementary Tables S4-S6. Troctolite-rich zones (TR) and magnetite-rich zones (M) within Unit 2 are indicated in the logs.

the granite-gneiss basement. Assimilation of dolomite would have promoted co-crystallisation of clinopyroxene with orthopyroxene to form the observed websterites; analogous to some of the hybrid rocks found at the contact between the Platreef and the Malmani Group at Sandsloot and Zwartfontein (Harris and Chaumba, 2001; McDonald et al., 2005). The presence of recrystallized domains of fine-grained pyroxenite and websterite (Fig. 7) within medium-grained equivalents suggest that later pulses of magma may have assimilated earlier (chilled) parts of the intrusion as autoliths. The generally medium-grain size of the ultramafic rocks, coupled with the presence of autoliths and the sharp and cross-cutting nature of any leuco-gabbronorites, all suggest that Unit 1 represents a relatively thin intrusion that cooled quickly and was perhaps already solidified when it was intruded and disrupted by a more evolved magma that formed the gabbronorites and leucogabbronorites of Unit 2.

On these grounds, the contentions of Maier et al. (2008) that both the PGE-poor ultramafic and the leucocratic PGE-rich rocks at Aurora represent a lateral strike equivalent of the Platreef (sensu stricto) or a contact-style of mineralisation linked to country rock assimilation are untenable. An alternative explanation must be sought.

8.2. Stratigraphic correlation

8.2.1. The significance of inverted pigeonite

The development of pigeonite (inverted to orthopyroxene) alongside orthopyroxene within the leuco-gabbronorites of Unit 2, and particularly in association with units that host high grade mineralisation (Fig. 6) is a key finding of this study. Manyeruke (2007) first reported the presence of inverted pigeonite in parts of what he considered "Platreef" as well as in "Main Zone" gabbronorites, but did not draw any further conclusions from these observations. Pigeonite is a characteristic mineral of the Main Zone of the Bushveld elsewhere (Atkins, 1969; Eales and Cawthorn, 1996; Nex et al., 2002). Pigeonite is absent from the lower portion of Unit 2 in both LAP-29 and LAP-31, and only begins to appear in the middle of this unit (Fig. 6). The first appearance is always as irregular pigeonite rims around cores of orthopyroxene crystallized between cumulus plagioclase (Fig. 8c). Pigeonite also develops as rims around orthopyroxene in olivine-rich zones (Fig. 8d). These observations suggest that the earliest pigeonite forms via replacement/reaction between primary orthopyroxene and residual melt prior to inverting; a relationship recognised in the Main Zone elsewhere in the northern limb (der Merwe M.J., 1978; Hulbert, 1983). Reverse textural relationships are developed in Unit 3, where cumulus pigeonite forms irregular cores that are rimmed by primary orthopyroxene (Fig. 8e and f–b). In Unit 3, the liquid composition has changed to the point where pyroxenes crystallize before plagioclase and pigeonite is the first pyroxene to crystallize on the liquidus before becoming resorbed and mantled by orthopyroxene.

Regardless of the crystallisation order, the rocks from the middle of Unit 2 upwards preserve both pigeonite and orthopyroxene. This finding is highly significant when one considers the mineral crystallisation sequence through the Main and Upper Zones in the northern limb as

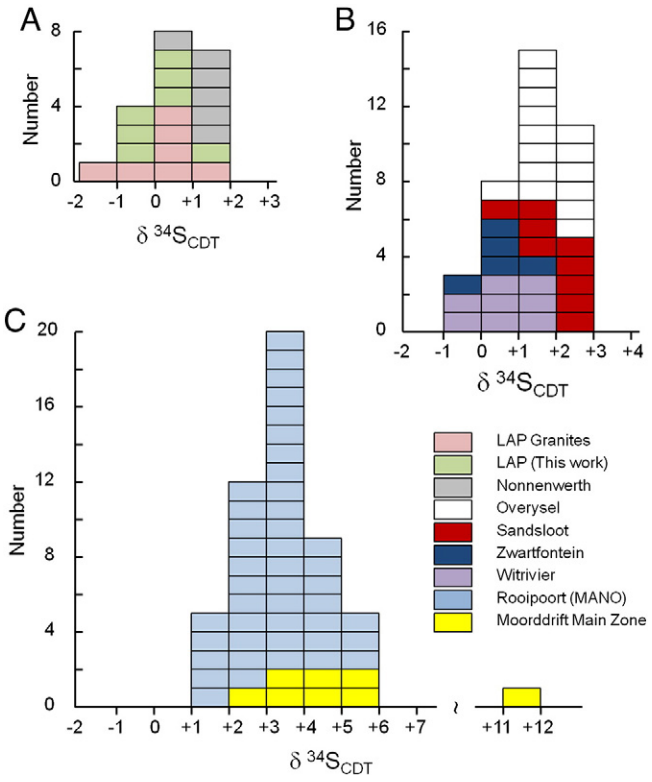

Fig. 15. Sulphur isotopes in leucogabbronorites and-gabbronorites La Pucella (this work) compared with other samples from the northern limb. La Pucella granites (Holwell et al., 2007); leucogabbronites at Nonnenwerth (Manyeruke, 2007), Platreef pyroxenites from Witrivier, Sandsloot, Overysel and Zwartfontein (Holwell et al., 2007); Mottled Anorthosite Unit at Rooipoort (Maier et al., 2008, Smith et al., 2014); and Moordrift (Holwell et al., 2013).

recorded in the Moordkopje (MO1) and Bellevue (BV1) boreholes (Ashwal et al., 2005; Roelofse and Ashwal, 2012). With the exception of one sample of Main Zone leucogabbro 100 m above the Platreef (Roelofse and Ashwal, 2012), pigeonite and orthopyroxene only occur together continuously and without cumulus magnetite over a narrow interval of ~200 m in the Upper Main Zone between depths of 2000–2200 m (Ashwal et al., 2005) in the BV1 borehole. This is strong evidence that the Aurora mineralisation may have developed within this interval during crystallisation of the northern Main Zone.

8.2.2. Mineral chemistry and stratigraphy

Major and trace element compositions of plagioclase and pyroxene in Units 2 and 3 in LAP-29 and LAP-31 are compared with data from the Upper Main Zone and the Upper Zone in the Bellevue BV1 borehole (Ashwal et al., 2005; Tanner et al., 2014) in Fig. 16. The range of plagioclase compositions at Aurora include the range from $An_{58–62}$ expected for rocks containing both orthopyroxene and inverted pigeonite (Fig. 16) but also extends to more Ca-rich compositions. The lower limit for An-content excludes most rocks from depths above 2000 m at Bellevue. Mg# values in low-Ca pyroxene and clinopyroxene at La Pucella encompass the expected ranges for much of the Upper Main Zone and the bottom half of the Upper Zone (800–2400 m depth) at Bellevue, but always include the key interval where orthopyroxene and inverted pigeonite are expected (Fig. 16). Trace elements have more restricted compositional ranges and are more useful for comparison. Concentrations of Sr and Ba in plagioclase at Aurora are most similar to the lower half of the Upper Main Zone at Bellevue and exclude most rocks above a depth of 2000 m (Fig. 16). Ni and Mn in low-Ca pyroxene exclude the bottom portion of the Upper Main Zone and the Troctolite Unit and are most consistent with rocks from depths between 1300 and 2300 m in the Bellevue core (Fig. 16).

Taken together, the major and trace element signatures in plagioclase and low-Ca pyroxene at Aurora most consistently match the part of the Upper Main Zone from 2000 to 2400 m depth at Bellevue. Significantly, this interval encompasses the first transition from pigeonite-free to pigeonite-bearing rocks and supports a direct correlation between these sequences (see Fig. 17). This differs from the initial model proposed by McDonald and Harmer (2010) that the Aurora rocks were the lateral equivalent of the Troctolite Unit at the base of the Bellevue borehole.

8.2.3. Magnetite-rich rocks

One magnetite gabbro unit occurs within Unit 2 in LAP-29 two occur in LAP-31 (Fig. 6). Magnetite is cumulus, surrounded by pyroxene, plagioclase and sulphides; relationships that characterise Upper Zone rocks and on the face of it, contradict the conclusions reached from mineral chemistry above. The presence of highly sodic plagioclase (as low as $An_{38–40}$), lithophile trace element profiles (Fig. 10) and high concentrations of incompatible elements (including P_2O_5 concentrations up to 0.29 wt%; >10 times those encountered in the leucogabbronorites - Table 1) confirm a highly evolved composition. The magnetite-rich zones are more coarse-grained (verging on pegmatoidal) compared with the leucogabbronorites above and below. They lack the highly calcic plagioclase ($An_{88–90}$), low P_2O_5 (<0.05 wt%), low Al_2O_3 (<2.5 wt%), low Sr (<35 ppm) and high Cr contents (>995 ppm) that characterise intrusive iron-rich ultramafic pegmatoid (IRUP) bodies that occur in the Main and Critical Zones throughout the Bushveld Complex (Scoon and Mitchell, 1994; Reid and Basson, 2002).

The presence of a lower magnetite gabbro with a troctolite above in both boreholes (Fig. 6) is suggestive that these may correlate along strike. However the lower magnetite gabbros are different thicknesses (<1 m in LAP-29 versus 4.5 m in LAP-31) and the upper magnetite gabbro developed in LAP-31 is missing from LAP-29 so it seems unlikely that these zones are completely stratiform. Our preferred interpretation for the general increase in all incompatible elements along with Fe is that they represent discontinuous zones of accumulated fractionated Fe-rich liquid within the cumulate rocks of Unit 2. Crystallisation of magnetite from the fractionated liquid may have triggered local sulphide immiscibility but because the sulphide liquid was not able to interact with any significant volume of melt, the low R factor only produced low tenor sulphides and low bulk rock PGE concentrations (Table 2; Fig. 13c).

8.3. Wider significance and possible relationships with other Main Zone-hosted mineralisation

If the Aurora mineralisation is located stratigraphically within the Upper Main Zone, a number of logical questions arise. First, could it extend to other areas of the northern limb? And second, does it reveal anything about the potential for Ni-Cu-PGE mineralisation hosted by Main Zone rocks elsewhere in the Bushveld Complex?

Ashwal et al. (2005) recorded an increase in the number of opaque minerals around 2100 m depth in the Bellevue core but did not specify whether these were sulphides or oxides. The top portion of the Upper Main Zone and the Upper Zone were analysed for S, Ni, Cu and PGE by Barnes et al. (2004). These authors found that this whole sequence was characterised by strong chalcophile element depletion and high Cu/Pd ratios (10^4–10^6). They used this to infer that the whole Upper Zone and (at least) the upper portion of Main Zone had been depleted in PGE; this loss was ascribed to removal during formation of the Platreef and the stratiform PGE reefs in the Critical Zone. Our data from Unit 3 shows the same geochemical signature of PGE depletion, evidently not from the Platreef but from the Aurora mineralisation directly below. Barnes et al. (2004) did not consider a major mineralisation event in the Main Zone and all of their Upper Main

Zone samples had Pd below the limit of detection (<1.4 ppb) with the deepest samples they analysed from 1973 m depth having minimum Cu/Pd ratios from 39,000 to 200,000. These Pd concentrations and Cu/Pd values are similar to those recorded in the pigeonite gabbronorites of Unit 3 at La Pucella (Fig. 13) and by Manyeruke (2007) in the upper gabbronorites at Nonnenwerth.

To our knowledge, no samples between 1973 m depth and the base of the Bellevue core at 2950 m have been analysed for PGE. An obvious test for the suggested correlation between Aurora and the middle portion of the Upper Main Zone at Bellevue (Fig. 17) would be systematic analyses for PGE, Ni and Cu through the interval from 2000 to 2400 m depth. This is given added impetus by the analyses of 4 gabbronorites collected from surface within this part of the Upper Main Zone by der Merwe M.J. (1978) which revealed a strong enrichment in Cu and S compared with Main Zone rocks located stratigraphically above and below.

It is also important to note that this prospective interval is not associated with any of the three new pulses of mafic magma into the northern limb proposed by Tanner et al. (2014) on the basis of reversals in the Cr content of low-Ca pyroxene. The pigeonite-orthopyroxene zone is located ~300 m above the first input close to the top of the Troctolite Unit at 2800 m and immediately below the second input inferred to have taken place at ~1980 m depth (Tanner et al., 2014). This stratigraphic position, coupled with the lack of evidence for any obvious reversals in mineral chemistry associated with the mineralized interval (Fig. 14), would tend to argue against a direct role for new mafic magma in the genesis of the mineralisation.

In-situ PGE mineralisation in Main Zone rocks is only known from two other localities and is restricted to the northern limb: on the farm Moorddrift in the far south, and on the Waterberg Project in the far north (Fig. 1). The geochemistry, mineralogy and S isotope characteristics of the mineralisation at Moorddrift have been described by Maier and Barnes (2010) and Holwell et al. (2013). The highest PGE grades are associated with a zone of gabbronorites, leucogabbronorites (mottled anorthosites) and one or more pyroxenites. The mineralisation is notably Pt-rich compared to other PGE deposits in the northern limb and Maier and Barnes (2010) correlated one pyroxenite with the well-known Pyroxenite Marker that is developed across the eastern and western Bushveld. They proposed that the Moorddrift mineralisation was stratigraphically linked with formation of the Pyroxenite Marker through a process linked to downward injection of crystal slurries in response to slumping of unconsolidated crystals towards the centre of the Bushveld Complex. Holwell et al. (2013) questioned this correlation and the complexity of the slumping model and consider the stratigraphic position of the Moorddrift mineralisation as uncertain because it is complicated by brecciation. Sulphur isotopes at Moorddrift are clearly different to Aurora (Fig. 15) and indicate different sources of S for the two deposits, regardless of whether they formed at the same time.

Maier and Barnes (2010) and Holwell et al. (2013) did not report inverted pigeonite at Moorddrift. Re-examination of thin sections of samples studied by Holwell et al. (2013) reveals that inverted pigeonite is apparently absent from samples from above, within and below the reef interval. Cumulus clinopyroxene dominates over lesser amounts of intercumulus orthopyroxene that is preferentially replaced by chlorite in the reef. The absence of pigeonite, coupled with the elevated Pt/Pd ratios and heavier S isotopes are inconsistent with any direct stratigraphic or genetic link between Moorddrift and Aurora.

The Waterberg mineralisation has an age within error with the rest of the Bushveld Complex (Huthmann et al., 2016) and is concentrated in two principal ore zones: at the base (F Zone) hosted by troctolites, harzburgites and pyroxenites; and in a zone of gabbronorites, pyroxenites and anorthosites (T Zone) close to what has been inferred as the boundary between the Main Zone and the Upper Zone. The T Zone contains upper and lower mineralized units designated T1 and T2 respectively (Lomberg, 2012, 2013).

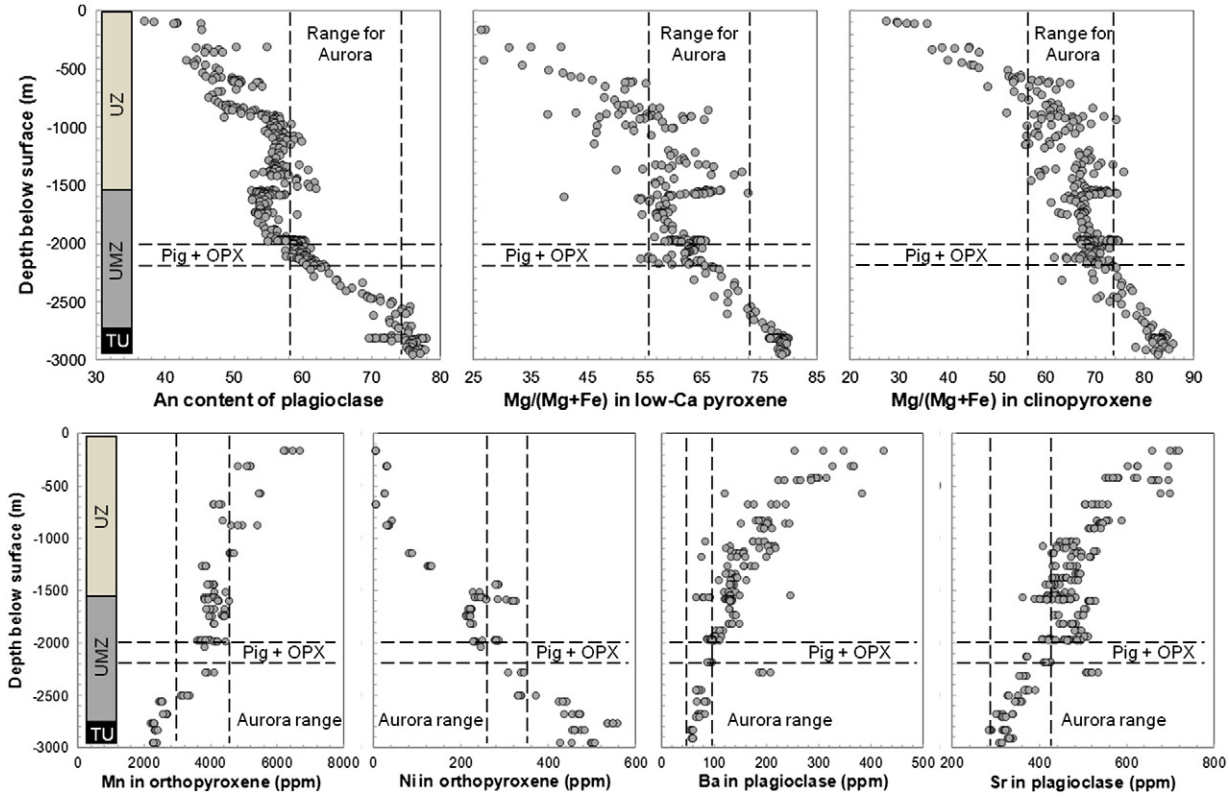

Fig. 16. Ranges of major element ratios and trace element concentrations in low-Ca pyroxene, clinopyroxene and plagioclase at La Pucella (shown by vertical dashed lines). These are compared with mineral compositions from the Bellevue BV1 borehole from Ashwal et al. (2005)and Tanner et al. (2014). This comprises the Troctolite Unit (TU), Upper Main Zone (UMZ) and Upper Zone (UZ). The part of the Upper Main Zone where pigeonite and orthopyroxene occur together is indicated by horizontal lines.

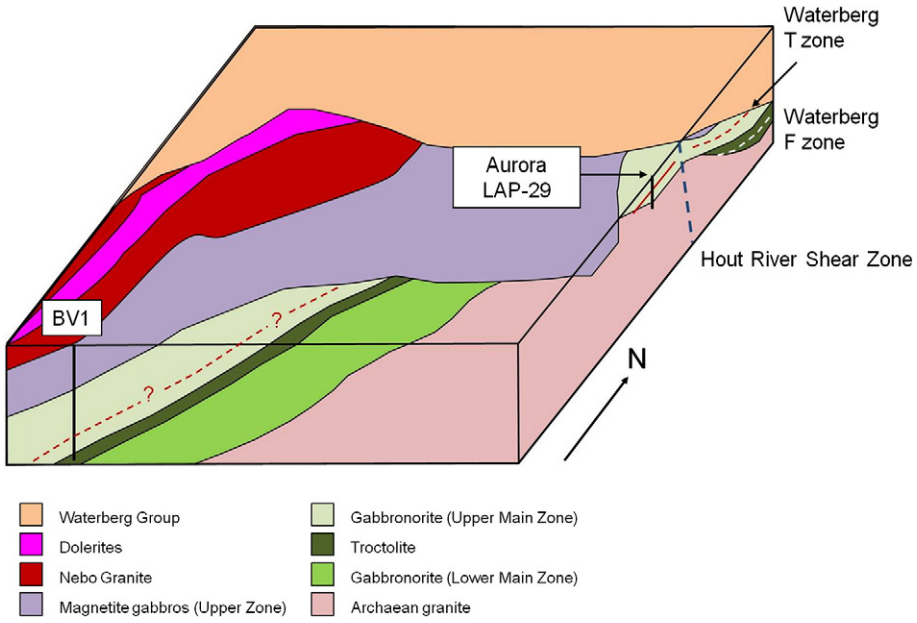

Fig. 17. Block diagram showing the suggested relationships between the mineralized rocks at Aurora compared with the Waterberg deposit and the Upper Main Zone above the Troctolite Unit.

The mineral resource estimates published by Lomberg (2012) indicate that the F Zone has Ni/Cu >1, a Pt/Pd ratio close to 0.5 and a (Pt + Pd) / Au ratio > 20. These characteristics are similar to some Platreef localities (Fig. 4) although it is not clear how much of the total Ni reported for the F Zone is hosted by olivine as opposed to sulphide. In contrast, the T Zone resource has Ni/Cu <1, a higher Pt/Pd ratio (0.6) and is richer in Au ((Pt + Pd) / Au ~4) and falls in the same cluster as Aurora (Fig. 4). McCreesh et al. (2015) highlighted the fact that that the T Zone was generally Cr-poor while the F zone was Cr-rich. These authors also reported the presence of inverted pigeonite in the gabbronorite host rock for the T2 unit. Sulphur isotopes in the T Zone are close to 0‰, similar to Aurora. There is a greater range in the F Zone ($\delta^{34}S = -3.5$ to +3‰), with a mean close to +1‰, possibly reflecting some input of crustal S close to the base of the intrusion (McCreesh et al., 2015). Taken together, these observations suggest the likelihood of a link between Aurora and the Waterberg T Zone (Fig. 17). More detailed work that emerges from studies at the Waterberg Project will prove or disprove this suggestion.

Considering the potential for mineralisation outside the northern limb, it is significant that Wilhelm et al. (1997) found widespread soil geochemistry anomalies for Ni, Cu, Pt, Pd and Au in the western limb of the Bushveld around Rustenburg, including a sporadically developed zone that appeared to parallel the Upper Main Zone in this part of the complex. These authors suggested that there may be a mineralized reef in the Upper Main Zone and suggested that similar anomalies could be found at the same level in other parts of the Bushveld Complex. To date there have been no confirmed reports of in-situ mineralisation from the Main Zone in the western limb and analyses of the Pyroxenite Marker in the eastern and western Maier et al. (2001) failed to find any significant enrichment in PGE. Early exploration at the Aurora Project focussed on the use of soil geochemistry and Cu anomalies were used to define the potential extent of the mineralisation. However the question of how the western Bushveld soil anomaly identified by Wilhelm et al. (1997) might relate to the mineralisation at Aurora remains open.

8.4. Genesis of the Aurora mineralisation

The mantle-like S isotope signatures and the high PGE tenors at Aurora (Fig. 12) are inconsistent with contact-style mineralisation involving in-situ contamination as an ore-triggering mechanism, even where that contamination involved the peridotite-gabbronorite unit. Naldrett (2005) originally proposed that Aurora-type mineralisation resulted from assimilation and re-melting of sulphides from earlier pyroxenites that he equated with a northern facies of the Platreef. There are several observations that argue against this interpretation. First, the ultramafic rocks at Aurora comprise only a small portion of the stratigraphy and the highest PGE grades consistently occur in the leucogabbronorites - at least 150 m above the uppermost melagabbronorite. It is difficult to envisage a mechanism whereby sulphide liquids formed by in-situ melting from the latter unit would become transported so far upwards. By way of comparison, a thin zone of "cannibalised" Platreef sulphide is present in the Main Zone above the Platreef (Holwell et al., 2005) but this is restricted to a few metres at the very base, directly above the Platreef contact. Secondly, the Ni/Cu ratios and PGE signatures of the two units are completely different, especially for veins and layers of leuco-gabbronorite within the peridotite-melagabbronorites (Fig. 12).

The presence of calc-silicate xenoliths and/or rafts at all levels of the stratigraphy at Aurora (Figs. 5 and 6) suggest that the magmas were progressively intruding into dolomites of the Malmani Subgroup. We suggest a process whereby the peridotite-melagabbronorite unit cooled quickly and formed a floor. New sulphide-bearing Main Zone magma intruded into and against this floor and the Malmani dolomite roof (Fig. 17). The available mineral chemistry and isotope data effectively rule out addition of new mafic magma or significant addition of external (isotopically heavy) sulphur from the shale-dominated members of the Pretoria Group.

In our view a plausible genetic model for Aurora is likely to involve separation of sulphide liquid(s) during formation of the Upper Main Zone. The absence of any enhanced Cr content in pyroxene coincident with the mineralisation (Fig. 14) precludes sulphide precipitation triggered by a new input of mafic magma, and instead sulphide saturation could have been achieved via fractional crystallisation, which would also explain the relatively Cu and Au-rich nature of the BMS. It would be expected that S and Au concentrations and the Cu/Ni and PPGE/IPGE ratios of the Main Zone magma would progressively increase, due to removal of Ni and IPGE into pyroxenes during formation of the Lower Main Zone, Troctolite Unit and the cumulates immediately

above - until sulphide saturation was reached. If the links between Aurora, the T Zone at Waterberg, and the Main Zone immediately above the Troctolite Unit suggested in Fig. 17 are confirmed then this potentially opens up an enormous area for new Ni-Cu-PGE exploration. The mapping work carried out by Holwell et al. (2005) and Holwell and Jordaan (2006) firmly established a break in time between the Platreef and the Main Zone, implying that the Main Zone magma would carry an intact, un-scavenged, metal budget into the chamber. This relationship is fundamentally different from the interaction between Main Zone and Upper Critical Zone magmas and crystals invoked to explain elemental and isotopic profiles across the Merensky and Bastard cyclic units in the eastern and western limbs (e.g. Seabrook et al., 2005). In our view, this difference has been under appreciated and is likely to be a major factor controlling the greater development of Main Zone-hosted PGE mineralisation in the northern limb compared with the other limbs of the Bushveld Complex.

9. Conclusions

This study has highlighted several key observations that distinguish the Ni-Cu-PGE mineralisation on the Aurora Project from that found in the Platreef and the stratiform reefs of the Critical Zone. Most importantly, sulphide mineralisation is concentrated in leucocratic rather than the melanocratic units that characterise all of the other PGE deposits of the Platreef and the Upper Critical Zone. The most PGE-enriched zones at Aurora are hosted by rocks that contain both inverted pigeonite and orthopyroxene and these are overlain by pigeonite gabbronorites that are strongly depleted in chalcophile elements.

Previous suggestions that Aurora represents a strike extension of the Platreef (Naldrett, 2005; Maier et al., 2008) are untenable and can be discounted on the basis of lithological associations, host mineralogy, and lithophile and PGE geochemistry. The mineral associations and the plagioclase and pyroxene compositions at Aurora most closely match that portion of the Upper Main Zone above the Troctolite Unit recognised and mapped by Van der Merwe (1976; 1978). We propose that Aurora may be a lateral equivalent (effectively a marginal facies) to this part of the Main Zone where PGE mineralisation may also be developed (Fig. 17). Outcrop samples from the Main Zone in the central part of the northern limb have anomalous enrichment in Cu (der Merwe M.J., 1978) whereas samples stratigraphically above this level in the BV1 borehole have high Cu/Pd ratios that are indicative of strong chalcophile element depletion (similar to the pigeonite gabbronorites of Unit 3). Proposed links between Aurora and mineralisation hosted within Main Zone rocks at Moorddrift are seen as unlikely on the basis of mineralogy, PGE geochemistry and S isotopes. Stronger similarities exist with the T Zone mineralisation that forms the upper mineralized zone of the Waterberg Project and we suggest that the T Zone could be an extension of the Aurora mineralisation, with higher average PGE grades, across the Hout River Shear Zone (Fig. 17).

As a consequence, we propose that Aurora could represent the marginal facies of a much more extensive zone of Upper Main Zone-hosted Ni-Cu-PGE mineralisation. This potentially mineralized zone above the Troctolite Unit is exposed on surface for at least 25 km of strike across the northern limb and much further if the correlation with the T Zone at Waterberg is upheld. This zone offers the potential for significant new discoveries of shallow Cu-Ni-PGE resources that could potentially be mined using open pit methods.

Supplementary data to this article can be found online at http://dx.doi.org/10.1016/j.oregeorev.2016.09.016.

Acknowledgements

This study was initiated in 2004 when the second author was Exploration Manager with Pan Palladium Limited. We thank the management of Pan Palladium, especially Jackie Van Schalkwyk for access to samples and for permission to publish the assay data from La Pucella shown in Fig. 6, and Eric Roodt for facilitating further sampling of LAP-04. Some initial sample preparation and analyses that contributed to this study were performed by Cardiff MESci students Steve Beckwith and Zoe Smithers. Sulphur isotope analyses were carried out by Alison MacDonald at the Scottish Universities Environmental Research Centre as part of NERC Isotope Geoscience Facilities Committee award IP/909/0506. We thank Pete Fisher for help with SEM analyses, and Tony Oldroyd and Lawrence Badham for preparation of thin sections. HSRH is sponsored by the Claude Leon Foundation. This work benefited from discussions with Paul Armitage, Marian Tredoux, Johan Kruger, Luke Longridge and Dominque Tanner. Ed Mathez and Freddie Roelofse provided insightful and constructive reviews, and Associate Editor Peter Lightfoot added further suggestions, that helped to improve the paper. We thank them all for their input.

References

Ashwal, L.D., Webb, S.J., Knoper, M.W., 2005. Magmatic stratigraphy in the Bushveld Northern Lobe: continuous geophysical and mineralogical data from the 2950 m Bellevue drillcore. S. Afr. J. Geol. 108, 199–232.
Atkins, F.B., 1969. Pyroxenes of the Bushveld intrusion, South Africa. J. Petrol. 10, 222–249.
Barnes, S.-J., Maier, W.D., 2002. Platinum-group elements and microstructures of normal Merensky Reef from Impala Platinum Mine, Bushveld Complex. J. Petrol. 43, 103–128.
Barnes, S.-J., W.D., M., L.D., A., 2004. Platinum-group elements in the Upper Zone of the Bushveld Complex. Chem. Geol. 208, 293–317.
Barnes, S.-J., Maier, W.D., Curl, E.A., 2010. Composition of the marginal rocks and sills of the Rusterburg layered suite, Bushveld Complex, South Africa: implications for the formation of the platinum-group element deposits. Econ. Geol. 105, 1491–1511.
Buchanan, D.L., Rouse, J.E., 1984. Role of contamination in the precipitation of sulphides in the platreef of the Bushveld Complex. In: D.L., B., Jones, M.J. (Eds.), Sulphide Deposits in Mafic and Ultramafic Rocks. Institution of Mining & Metallurgy, London, pp. 141–146.
Bye, A.R., Bell, F.G., 2001. Stability and slope design at Sandsloot open pit, South Africa. Int. J. Rock Mech. Min. Sci. 38, 449–466.
Cawthorn, R.G., 2002. Delayed accumulation of plagioclase in the Bushveld Complex. Mineral. Mag. 66, 881–893.
van der Merwe M.J., 1978. The geology of the basic and ultramafic rocks of the Potgietersrus Limb of the Bushveld Complex: Unpublished PhD thesis, University of the Witwatersrand, 176 p.
Eales, H.V., Cawthorn, R.G., 1996. The Bushveld Complex. In: Cawthorn, R.G. (Ed.), Layered Intrusions. Elsevier Science, pp. 181–230.
Gain, S.B., Mostert, A.B., 1982. The geological setting of the platinoid and base metal sulfide mineralisation in the Platreef of the Bushveld Complex in Drenthe, north of Potgietersrus. Econ. Geol. 77, 1395–1404.
Harmer, R.E., Pillay, N., Davis, P.G., 2004. The Aurora project - Main Zone hosted PGE-base metal mineralisation at the northern outcrop limit of the Bushveld northern limb, north of Mokopane. 1st Platreef Workshop Field Guide, Mokopane 16–19 July 2004Geoscience Africa. University of the Witwatersrand.
Harris, C., Chaumba, J.B., 2001. Crustal contamination and fluid-rock interaction during the formation of the Platreef, Northern Limb of the Bushveld Complex, South Africa. J. Petrol. 42, 1321–1347.
Holwell, D.A., 2006. The roles of magmatism, contamination and hydrothermal processes in the development of Platreef mineralisation, Bushveld Complex, South Africa. Unpublished PhD thesis, Cardiff University, 285 pp.
Holwell, D.A., Jordaan, A., 2006. Three-dimensional mapping of the Platreef at the Zwartfontein South mine: implications for the timing of magmatic events in the northern limb of the Bushveld Complex, South Africa. Appl. Earth Sci. (Trans. Inst. Mining Metall. B) 115, 41–48.
Holwell, D.A., McDonald, I., 2006. Petrology, geochemistry and the mechanisms determining the distribution of platinum-group element and base metal sulfide mineralisation in the Platreef at Overysel, northern Bushveld Complex, South Africa. Mineral. Deposita 41, 575–598.
Holwell, D.A., Armitage, P.E.B., McDonald, I., 2005. Observations on the relationship between the Platreef and its hangingwall. Appl. Earth Sci. (Trans. Inst. Mining Metall. B) 114, B199–B207.
Holwell, D.A., Boyce, A.J., McDonald, I., 2007. Sulfur isotope study of the Platreef, northern Bushveld Complex: genetic implications for the origin of sulfide mineralisation. Econ. Geol. 102, 1091–1110.
Holwell, D.A., Jones, A., Smith, J.W., Boyce, A.J., 2013. New mineralogical and isotopic constraints on main zone-hosted PGE mineralisation at Moorddrift, northern Bushveld Complex. Mineral. Deposita 48, 675–686.
Huber, H., Koeberl, C., McDonald, I., Reimold, W.U., 2001. Geochemistry and petrology of Witwatersrand and Dwyka diamictites from South Africa: search for an extraterrestrial component. Geochim. Cosmochim. Acta 65, 2007–2016.
Hughes, H.S.R., Boyce, A.J., McDonald, I., Davidheiser-Kroll, B., Holwell, D.A., MacDonald, A., Oldroyd, A., 2015. Contrasting mechanisms for crustal sulphur contamination of mafic magma: evidence from dyke and sill complexes from the British Palaeogene Igneous Province. J. Geol. Soc. 172, 443–458.
Hulbert, L.J., 1983. A Petrographical Investigation of the Rustenburg Layered Suite and Associated Mineralisation south of Potgietersrus. Unpublished DSc dissertation, University of Pretoria, 511 p.

Hutchinson, D., Foster, J., Prichard, H.M.P., Gilbert, S., 2015. Concentration of particulate platinum-group minerals during magma emplacement; a case study from the Merensky Reef, Bushveld Complex. J. Petrol. 56, 113–159.
Huthmann, F.M., Yudovskaya, M.A., Frei, D., Kinnaird, J.A., 2016. Geochronological evidence for an extension of the Northern Lobe of the Bushveld Complex, Limpopo Province, South Africa. Precambrian Res. 280, 61–75.
Kinnaird, J.A., McDonald, I., 2005. An introduction to the mineralisation in the northern limb of the Bushveld Complex. Appl. Earth Sci. (Trans. Inst. Mining Metall. B) 114, B194–B198.
Kinnaird, J.A., Nex, P.A.M., 2015. An overview of the Platreef. In: Hammond, N.Q., Hatton, C. (Eds.), "Platinum-Group Element (PGE) Mineralisation and Resources of the Bushveld Complex, South Africa", Mineral Resources Series Number 2 Vol. 5. Council for Geoscience, Pretoria, pp. 193–342.
Kinnaird, J.A., Hutchinson, D., Schürmann, L., Nex, P.A.M., de Lange, R., 2005. Petrology and mineralisation of the southern Platreef: northern limb of the Bushveld Complex, South Africa. Mineral. Deposita 40, 576–597.
Kruger, F.J., 2005. Filling the Bushveld Complex magma chamber: lateral expansion, floor interaction, magmatic unconformities and giant chromitite and PGE deposits. Mineral. Deposita 40, 451–472.
Lee, C.A., 1996. A review of mineralisation in the Bushveld Complex and some other layered mafic intrusions. In: Cawthorn, R.G. (Ed.), Layered Intrusions. Elsevier Science, pp. 103–146.
Lomberg, K., 2012. Updated exploration results and mineral resource estimate for the Waterberg platinum project, South Africa. (Latitude 23° 21′ 53″S, Longitude 28° 48′ 23″E). NI-43-101 Report Prepared for Platinum Group Metals Ltd by Coffey Mining, 1st September 2012 89pp.
Lomberg, K., 2013. Revised and Updated mineral resource estimate for the Waterberg platinum project, South Africa. (Latitude 23° 21′ 53″S, Longitude 28° 48′ 23″E). NI-43-101 Report Prepared for Platinum Group Metals Ltd by Coffey Mining, 1st February 2013 98pp.
Maier, W.D., Barnes, S.-J., 2010. The petrogenesis of platinum-group element reefs in the upper Main Zone of the Northern lobe of the Bushveld Complex on the farm Moorddrift, South Africa. Econ. Geol. 105, 841–854.
Maier, W.D., Barnes, S.-J., van der Merwe, M.J., 2001. The concentrations of PGE in the pyroxenite marker, Bushveld Complex: implications for the formation of the Main Zone. S. Afr. J. Geol. 104, 335–342.
Maier, W.D., Barnes, S.-J., Teigler, B., de Klerk, W.J., Mitchell, A.A., 1996. Cu/Pd and Cu/Pt of silicate rocks in the Bushveld Complex: implications for platinum-group element exploration. Econ. Geol. 91, 1151–1158.
Maier, W.D., De Klerk, L., Blaine, J., Manyeruke, T., Barnes, S.-J., Stevens, M.V.A., Mavrogenes, J.A., 2008. Petrogenesis of contact-style PGE mineralisation in the northern lobe of the Bushveld Complex: comparison of data from the farms Rooipoort, Townlands, Drenthe and Nonnenwerth. Mineral. Deposita 43, 255–280.
Maier, W.D., Barnes, S.-J., Groves, D.I., 2013. The Bushveld Complex, South Africa: formation of platinum-palladium, chrome- and vanadium-rich layers via hydrodynamic sorting of a mobilized cumulate slurry in a large, relatively slowly cooling, subsiding magma chamber. Mineral. Deposita 48, 1–56.
Manyeruke, T.D., 2007. Geochemical Variation of the Platreef in the Northern Limb of the Bushveld Complex: Implications for the Origin of the PGE Mineralisation PhD thesis University of Pretoria 206pp.
Manyeruke, T.D., Maier, W.D., Barnes, S.-J., 2005. Major and trace element geochemistry of the Platreef on the farm Townlands, northern Bushveld Complex. S. Afr. J. Geol. 108, 381–396.
McCreesh, M.J.G., Kinnaird, J.A., Yudovskaya, M., 2015. A comparison of the two unique mineralised packages associated with Main Zone rocks in the Waterberg extension project of the Northern Limb, Bushveld Complex. Abstract, 6th Platreef Workshop, Mokopane, 8–10th May 2015, pp. 36–39.
McDonald, I., Harmer, R.E., 2010. The nature of PGE mineralisation in the Aurora Project area, northern Bushveld Complex, South Africa. Abstract, 11th International Platinum Symposium, 21st–24th June 2010, Sudbury, Ontario. In: Jugo, P.J., Lesher, C.M., Mungall, J.E. (Eds.), Ontario Geological Survey, Miscellaneous Release Data-269.
McDonald, I., Holwell, D.A., 2011. Geology of the Northern Bushveld Complex and the setting and genesis of the Platreef Ni-Cu-PGE deposit. In: Ripley, E., Li, C. (Eds.), Magmatic Ni-Cu and PGE Deposits: Geology, Geochemistry and Genesis: Reviews in Economic Geology, 17. Society of Economic Geologists, pp. 297–328.
McDonald, I., Viljoen, K.S., 2006. Platinum-group element geochemistry of mantle eclogites: a reconnaissance study of xenoliths from the Orapa kimberlite, Botswana. Appl. Earth Sci. (Trans. Ins. Mining Metall. B) 115, B81–B93.
McDonald, I., Holwell, D.A., Armitage, P.E.B., 2005. Geochemistry and mineralogy of the Platreef and "critical zone" cumulates of the Northern limb of the Bushveld Complex, South Africa: implications for Bushveld stratigraphy and the development of PGE mineralisation. Mineral. Deposita 40, 526–549.
McDonough, W.F., Sun, S.S., 1995. Composition of the earth. Chem. Geol. 120, 223–253.
Meurer, W.P., Boudreau, A.E., 1998. Compaction of igneous cumulates. Part I - Geochemical consequences for cumulates and liquid fractionation trends. J. Geol. 106, 281–292.
Mungall, J.E., Brenan, J.M., 2014. Partitioning of platinum-group elements and Au between sulfide liquid and basalt and the origins of mantle-crust fractionation of the chalcophile elements. Geochim. Cosmochim. Acta 125, 265–289.
Naldrett, A.J., 2005. The Platreef: death at Drenthe; resurrection at Aurora. Extended abstract volume. 2nd Platreef Workshop, Mokopane, South Africa, 28–30th October 2005.
Naldrett, A.J., Lehmann, J., 1988. Spinel non-stoichiometry as the explanation for Ni-, Cu-, and PGE-enriched sulphides in chromitites. In: H.M., P., P.J., P., J.F.W., B., S.J., C. (Eds.), Geo-Platinum 87. Elsevier Applied Science, London, pp. 113–143.
Nex, P.A.M., Cawthorn, R.G., Kinnaird, J.A., 2002. Geochemical effects of magma addition: compositional reversals and decoupling of trends in the Main Zone of the western Bushveld Complex. Mineral. Mag. 66, 833–856.
Reid, D.L., Basson, I.J., 2002. Iron-rich ultramafic pegmatite replacement bodies within the upper critical zone, Rustenburg layered suite, Northam platinum mine, South Africa. Mineral. Mag. 66, 895–914.
Roelofse, F., Ashwal, L.D., 2012. The Lower Main Zone in the Northern Limb of the Bushveld Complex: a 1·3 km thick sequence of intruded and variably contaminated crystal mushes. J. Petrol. 53, 1449–1476.
Scoon, R.N., Mitchell, A.A., 1994. Discordant iron-rich ultramafic pegmatites in the Bushveld Complex and their relationship to iron-rich intercumulus and residual liquids. J. Petrol. 35, 881–917.
Seabrook, C.L., Cawthorn, R.G., Kruger, F.J., 2005. The Merensky Reef, Bushveld Complex: mixing of minerals not mixing of magmas. Econ. Geol. 100, 1191–1206.
Smart, G.D., 2013. PGE in the Platreef: A Petrological and Geochemical Study of the Turfspruit Cyclic Unit on the Farm Turfspruit. Unpublished MESci dissertation, Cardiff University, p. 163.
Smith, J.W., Holwell, D.A., McDonald, I., 2014. Precious and base metal geochemistry and mineralogy of the Grasvally norite–pyroxenite–anorthosite (GNPA) member, northern Bushveld Complex, South Africa: implications for a multistage emplacement. Mineral. Deposita 49, 667–692.
South African Committee for Stratigraphy, 1980. Stratigraphy of South Africa, Part 1 (Compiler, L.E. Kent). Geological Survey of South Africa Handbook 8. Geological Survey of South Africa, Pretoria 690pp.
Tanner, D., Mavrogenes, J.A., Arculus, R.J., Jenner, F.E., 2014. Trace element stratigraphy of the Bellevue core, Northern Bushveld: multiple magma injections obscured by diffusive processes. J. Petrol. 55, 859–882.
van der Merwe, M.J., 1976. The layered sequence of the Potgietersrus limb of the Bushveld Complex. Econ. Geol. 71, 1337–1351.
van der Merwe, M.J., 2008. The geology and structure of the Rustenburg layered suite in the Potgietersrus/Mokopane area of the Bushveld Complex, South Africa. Mineral. Deposita 43, 405–419.
VanTongeren, J.A., Zirakparvar, N.A., Mathez, E.A., 2016. Hf isotopic evidence for a cogenetic magma source for the Bushveld Complex and associated felsic magmas. Lithos 248-251, 469–477.
Venmyn-Rand, 2010. Independent Technical Experts Report on the Mineral Assets of Sylvania Resources Limited – In the Form of a Competent Persons Report by Venmyn-Rand (Pty) Limited 151pp.
Westerlund, K.J., Gurney, J.J., Carlson, R.W., Shirey, S.B., Hauri, E.H., Richardson, S.H., 2004. A metasomatic origin for late Archean eclogitic diamonds: implications from internal morphology of diamonds and Re-Os and S isotope characteristics of their sulphide inclusions from the late Jurassic Klipspringer kimberlites. S. Afr. J. Geol. 107, 119–130.
White, J.A., 1994. The Potgietersrus Prospect - Geology and Exploration History. XVth CMMI Congress Vol. 3. SAIMM, Johannesburg, pp. 173–181.
Wilhelm, H.J., Zhang, H., Chen, F.L., Elsenbroek, J.H., Lombard, M., de Bruin, D., 1997. Geochemical exploration for platinum-group elements in the Bushveld Complex, South. Mineral. Deposita 32, 349–361.
Yudovskaya, M., Kinnaird, J., Naldrett, A.J., Mokhov, A.V., McDonald, I., Reinke, C., 2011. Facies variation in PGE mineralisation in the Central Platreef of the Bushveld Complex, South Africa. Can. Mineral. 49, 1349–1384.
Yudovskaya, M.A., Kinnaird, J.A., Sobolev, A., Kuzmin, D.V., McDonald, I., Wilson, A.H., 2013. Petrogenesis of the Lower Zone olivine-rich cumulates beneath the Platreef and their correlation with recognized occurrences in the Bushveld Complex. Econ. Geol. 108, 1923–1952.
Zeh, A., Ovtcharova, M., Wilson, A.H., Schaltegger, U., 2015. The Bushveld Complex was emplaced and cooled in less than one million years – results of zirconology, and geotectonic implications. Earth Planet. Sci. Lett. 418, 103–114.